Title: A local translation program regulates centriole amplification in the airway epithelium

Authors: Helu Liu[1,4], Huijun Li[1,4], Zhihua Jiang[1], Shibo Jin[2], Rui Song[2], Ying Yang[1], Jun Li[1], Jingshu Huang[1], Xiaoqing Zhang[1], Xuesong Dong[1], Jianwen Que[1], Munemasa Mori[1], Marvin J Fritzler[3], Lin He[2], Wellington Cardoso[1]*, and Jining Lu[1]*

Affiliations: 1. The Columbia Center for Human Development, Division of Pulmonary, Allergy & Critical Care Medicine, Department of Medicine, Columbia University, College of Physicians & Surgeons, New York, New York, United States of America
2. Division of Cellular and Developmental Biology, Department of Molecular & Cell Biology, University of California, Berkeley, Berkeley, California, USA.
3. Department of Biochemistry and Molecular Biology, Faculty of Medicine, University of Calgary, Canada.
4. These authors contributed equally: Helu Liu, Huijun Li.

***Corresponding authors:**

Wellington V. Cardoso MD, PhD.,
Professor of Medicine and Genetics and Development,
Director, Columbia Center for Human Development,
Pulmonary Allergy & Critical Care Medicine
Department of Medicine,
Columbia University Medical Center,
650 West 168th Street, BB 8-812
New York, NY 10032
wvc2104@cumc.columbia.edu

Jining Lü PhD.,
Program Director,
Division of Lung Diseases,
National Heart, Lung, and Blood Institute
National Institutes of Health,
6705 Rockledge Drive, Room 407-J, MSC 7952
Bethesda, MD 20892-7952
Email:jining.lu@nih.gov

Abstract

Biogenesis of organelles requires targeting of subset of proteins to specific subcellular domains by signal peptides or mechanisms controlling mRNA localization and local translation. How local distribution and translation of specific mRNAs for organelle biogenesis is achieved remains elusive and likely to be dependent on the cellular context. Here we identify Trinucleotide repeat containing-6a (*Tnrc6a),* a component of the miRNA pathway, distinctively localized to apical granules of differentiating airway multiciliated cells (MCCs) adjacent to centrioles. In spite of being enriched in TNRC6A and the miRNA-binding protein AGO2, they lack enzymes for mRNA degradation. Instead, we found these apical granules enriched in components of the mRNA translation machinery and newly synthesized proteins suggesting that they are specific hubs for target mRNA localization and local translation in MCCs. Consistent with this, *Tnrc6a* loss of function prevented formation of these granules and led to a broad reduction, rather than stabilization of miRNA targets. These included downregulation of key genes involved in ciliogenesis and was associated with defective cilia formation both in vivo and in primary airway epithelial cultures. Similar analysis of Tnr6a disruption in yolk sac showed stabilization of miRNA targets, highlighting the potential diversity of these mechanisms across organs.

Keywords: Trinucleotide repeat-containing 6A (*Tnrc6a*), Cytoplasmic RNP granules, mRNA subcellular localization, Local translation, Centriologenesis

Highlights:

1. *Tnrc6a* is selectively and abundantly present in multiciliated cells (MCC) of the lung.
2. Loss of *Tnrc6a* in the lung leads to reduction, not stabilization of miRNA targets.
3. TRNC6A concentrates in apically-localized granules adjacent to centrioles in MCCs.
4. Apically-localized granules contain AGO2, but lack mRNA degradation enzymes.
5. Newly-synthesized proteins and translation machinery components are concentrated or associated with apically localized granules.
6. *Tnrc6a* is required for efficient protein production of miRNA targets and proper centriole amplification during multicilia formation.

Introduction:

Biogenesis of subcellular organelles requires efficient delivery and concentration of subsets of proteins to specific intracellular sites for prompt assembly[1,2]. Targeting proteins to specific subcellular compartments with signal peptides or by translation of localized mRNAs is known to be involved in this process[3-5]. mRNA subcellular localization and local translation are evolutionary conserved and efficient mechanisms to create functional and structural asymmetries in cells by rapidly producing encoded proteins when and where required [2]. The prevalence and precise subcellular localization of certain mRNAs in association with specific organelles suggest a significant contribution of local translation[3]. Mechanisms generating asymmetric distribution of proteins in polarized cells are functionally relevant in regulating multiple aspects of cell behavior, including proliferation, migration and differentiation.

Centrioles are core structures of centrosomes involved in nucleation and formation of mitotic spindles critical for cell division[6]. Centrioles also function as basal bodies for the assembly of primary cilia and multicilia[6,7]. During multiciliogenesis, each differentiating multiciliated cell (MCC) generates several hundreds of centrioles. A number of mRNAs localize and concentrate in centrioles or centrosomes[3,8,9]. Concentration of proteins and mRNAs in centrosomes might be achieved by targeting actively translating polysomes [8]. In addition, centriolar proteins are suggested to recruit the protein translation machinery that regulates the translation of specific mRNAs[10]. Still, little is known about the mechanisms of mRNA localization and local translation in centriole amplification. It is also unclear how microRNAs contribute to this process.

Trinucleotide repeat containing 6a (TNRC6A) is a direct partner of Argonaute proteins (AGOs), which play a critical role in miRNA-induced mRNA degradation[11]. AGOs and TNRC6A have been reported in randomly-distributed cytoplasmic granules known as P-bodies, which are enriched in translation suppressors and mRNA degradation enzymes, but lack protein synthesis machinery[12]. TNRC6A and AGO2 can be also detected in other cytoplasmic ribonucleoprotein granules, such as stress granules and neuronal transport granules[13-15]. Cell culture studies show *Tnrc6a* present in most cell types, however analyses of developing and adult tissues in vivo show that levels of *Tnrc6a* expression can differ markedly[16,17].

In an effort to gain further insights into the tissue distribution and processes associated with *Tnrc6a* and miRNAs, here we identified *Tnrc6a* in the lung selectively and abundantly expressed in MCCs of conducting airways. We found TNRC6A protein asymmetrically distributed in these cells in a not previously identified population of apical granules, which also contained AGO2 . However these granules differed from P-bodies as they lacked mRNA degradation enzymes and instead were highly enriched in components of the mRNA translation machinery and newly-synthesized proteins. Loss of function of *Tnrc6a* prevented these granules from forming and resulted in broad reduction of miRNA targets, including key components of the centriole biogenesis machinery required for multicilia formation. Our study suggests that this novel class of TNRC6A-containing apical granules are local translation hubs required to mediate large-scale production of centriolar proteins in MCCs. Our data also supports the idea that key components of the miRNA pathway can be utilized for mRNA recruitment and localization required for local translation.

Results:

***Tnrc6a* is selectively expressed in multiciliated cells of the lungs.**

We have previously generated a *Tnrc6a*$^{gt/+}$ reporter mouse carrying a gene trap insertion of β-galactosidase in the *Tnrc6a* locus to investigate expression and function of *Tnrc6a* in mouse development[18]. In the process of further characterizing these mutants, we performed marker analysis and X-gal staining in the adult lungs and found a striking selective pattern of β-galactosidase activity in the airway epithelium (**Fig. 1a).** Little to no signals were present in the alveolar epithelium and overall in the mesenchymal compartment. This pattern was similarly observed for *Tnrc6a* as determined by in situ hybridization (**Fig. 1b).** Moreover, high levels of β-galactosidase activity co-labeled with acetylated α-tubulin (Ac-α-tub), indicated that *Tnrc6a* was selectively expressed in MCCs of the airway epithelium (**Fig. 1c)**. Immunofluorescence (IF) staining with the human index serum (termed as 18033), widely used for detection of TNRC6A protein[19,20], showed signals restricted to Ac-α-tub positive cells, further confirming selectivity to MCCs (**Fig. 1d)**. To examine when these granules appear during MCC differentiation, we performed immunostaining for TNRC6A (18033) and FOXJ1, an early marker of MCCs, in airway progenitors isolated from adult mouse trachea differentiating in air-liquid interface (ALI) cultures[21]. TNRC6A expression was first detected at ALI day2 in emerging FOXJ1+ cells. By day3-4, as these cells underwent large-scale centriole amplification to initiate multiciliogenesis[21], TNRC6A+ cytoplasmic granules became most abundant in MCCs (**Fig. 1e**). Signals then were reduced in subsequent days in more mature MCCs exhibiting abundant Ac-α-tub expression **(Fig. 1f).**

Disruption of *Tnrc6a* expression leads to reduction, rather than stabilization of miRNA targets in mutant lungs.

The distinctive pattern of *Tnrc6a* expression in the airway epithelium, particularly in MCCs, led us to investigate its potential role in the lung. In a previous study we showed that homozygous *Tnrc6a*$^{gt/gt}$ (hereafter *Tnrc6a* null) mice in a mixed genetic background have severe yolk sac defects and die around E9.5. However, we found that embryonic lethality can be prevented if these mutants are backcrossed for more than 10 generations with C57BL/6 mice. This strategy allowed us to investigate the impact of *Tnrc6a* in the developing lung, when the airway epithelium is undergoing differentiation and abundant MCCs are present. Thus, we performed global transcriptome analysis (Affymetrix GeneChip) in lungs from control and mutants at E18.5 (GSE89327). To examine the connection between miRNAs and *Tnrc6a*-regulated targets in the lung, we did gene set enrichment analysis (GSEA) using a gene set containing the most evolutionary conserved targets of 83 conserved miRNAs as determined by Targetscan (http://www.targetscan.org) (**Supplementary Figs. 1-2**), GSEA was also performed in the yolk sac array dataset (GSE30244) using this gene set. Consistent with the expected role of *Tnrc6a* in miRNA-mediated gene silencing[18,22,23], targets of most miRNAs (78 out of 83) were significantly enriched in the list of genes upregulated in *Tnrc6a* null yolk sacs**,** indicating a role for *Tnrc6a* in the destabilization of miRNA targets. Surprisingly, similar analysis using the *Tnrc6a* null lung array dataset (GSE89327) showed that targets of most miRNAs (79 out of 83) were enriched among the genes significantly reduced in *Tnrc6a* mutant lungs, but not among the genes upregulated. This unexpected finding suggested that, in the lung, *Tnrc6a* stabilizes miRNA targets instead of promoting degradation.

As demonstrated in other systems, genetic deletion of *Tnrc6a* disrupts miRNA function without affecting miRNA expression or stability[18,22]. This was also the case in our mutants. We

compared levels of miR-449 (from the miR34-449 cluster) and miR146, present in both MCC and yolk sac, and found no difference in expression between WT and *Tnrc6a* null mutants (**Supplementary Fig. 3)**[18]. Analysis of miR-34/449 predicted targets in both array datasets showed that, among 94 transcripts with conserved binding sites significantly altered in mutant lungs, the majority (80%) was downregulated (**Supplementary Fig. 2, pages 1-2)**. By contrast 75% of the conserved miR-34/449 targets altered in yolk sac mutants were upregulated (72 total) (**Supplementary Fig. 1, pages1-2)**. Interestingly, among the top 30 most downregulated genes in mutant lungs, several, such as *Rsph1* and *Spef2*, have been implicated in multicilia formation and 30% of these genes are predicted targets of miR-34/449, key in multiciliogenesis[23,24] (**Supplementary table 1, Supplementary Fig. 4**). We confirmed expression of Spef2 and Rsph1 in the lung in multiciliated cells and their signals reduced in *Tnrc6a*^{null} mutants compared to WT. qRT-PCR further confirmed the reduced expression of additional miR-34/449 targets, such as *Rnf213, Tmem159* and *Calcrl*, besides *Rsph1*, *Spef2* (**Supplementary Fig. 4a-c**). Together, our data strongly suggested that, in the lung, *Tnrc6a* was not involved in degradation of miRNA targets but rather appear to be required for the mRNA stabilization.

TNRC6A proteins concentrate in a novel class of apical epithelial granules that lack mRNA degradation enzymes.

We asked how TNRC6A could stabilize miRNA targets in lungs, while promoting miRNA target degradation in yolk sacs. To start addressing this question, we examined the subcellular localization of TNRC6A in these two tissues. IF of E9.5 yolk sacs with human index serum (18033) showed positive granules selectively present in the endodermal layer, consistent with our previous in situ hybridization and β-galactosidase staining (**Supplementary Fig. 5**)[18]. These granules were heterogeneous in size, randomly localized in the cytoplasmic and co-stained with AGO2, DCP1A, DDX6 and XRN1, components of the miRNA processing machinery present in P-bodies[25]. The data supported the idea that TNRC6A destabilizes miRNA targets in the yolk sac in vivo[18].

Human index serum (18033) staining of MCCs in ALI airway epithelial cultures showed signals in a similar heterogeneous population of randomly distributed cytoplasmic granules (P-bodies) in the yolk sac. However, it also identified a second population of granules more homogeneous in size apically-localized in MCCs. Immunostaining using the TNRC6A monoclonal antibody (4B6) labeled distinctly this class of apical granules and showed them localized underneath the multicilia of immature MCCs (**Fig. 2a-e)**. The presence of these apical granules in airways of E18.5 WT lungs, but not in *Tnrc6a* null lungs (**Supplementary Fig. 11b),** strongly supported the specificity of this antibody. We also found that these apical granules appeared in a dynamic fashion during differentiation, being most abundant in immature MCCs, diminishing in mature MCCs **(Fig. 1f).**

The human index serum (18033) is known to contain antibodies for both TNRC6A and EDC4, another key component of P-bodies[26]. To gain additional insights into the composition of the two classes of granules detected by human index serum we co-stained MCCs with both human index serum and EDC4 monoclonal antibody. Interestingly, EDC4 antibody detected the P-bodies, but not the apically-localized granules that we identified using the 4B6 antibody, supporting the distinct distribution of TNRC6A-containing granules (**Fig. 2e-f)**. To further confirm this observation, airway progenitor cells were transduced with a lentiviral vector expressing TNRC6A-EGFP fusion protein at the time of plating followed by differentiation into MCCs in ALI cultures[21]. We found TNRC6A-EGFP fusion proteins concentrated in granules relatively uniform in size and apically localized in MCCs (**Fig. 2g)**. The absence of EDC4 in these granules led us to examine additional P-bodies components. To our surprise, enzymes

and proteins needed for mRNA degradation, such as DCP1A, DDX6 and XRN1 were highly expressed in randomly localized P-bodies, but largely undetectable in the apical granules of the same MCC (**Fig. 2h, Supplementary Fig. 6**).

Together, our analyses of airway MCCs showed the existence of an apically-localized class of granules distinct from P-bodies enriched in TNRC6A protein and lacking the mRNA degradation enzymes present in P-bodies (**Fig. 2i)**. The discrepancy in the localization of TNRC6A proteins between airway MCCs and yolk sac endodermal cells might lead to the distinct function of TNRC6A in these two cell types in which TNRC6A is highly expressed.

Formation of apically-localized granules depend on the expression of miR-34/449.

TNRC6A is a known partner of AGO2[12,27]. Co-IF staining of human index serum with AGO2 showed the co-localization of AGO2 in both classes of granules in MCC (**Fig. 3a**). This was additionally confirmed by lentiviral transduction of AGO2-EGFP fusion protein in ALI cultures, which showed EGFP significantly enriched in the apical granules underneath the cilia (**Fig. 3b-c**). Next, we examined whether miRNAs previously reported in MCCs were enriched at the subcellular location where we found the TNRC6A-contaning apical granules. ISH showed that miR-449a, a miRNA known to be critical for multiciliogenesis [23,24,28,29], was enriched apically, adjacent to the base of multicilia (**Fig. 3c-d**). ISH signals were also detected apically for other miRNAs reported in MCCs, such as miR-34a and miR-34b (**Supplementary Fig. 7)**. Thus, the apical granules contained TNRC6A, AGO2, miRNAs and presumably their targets.

Next, we asked whether formation of these granules depended on miR-34/449, a family of miRNAs abundantly expressed in MCCs, crucial for basal body maturation and apical docking[23]. For this we examined ALI airway epithelial cultures from miR-34/449 null mice in which all three loci encoding miR-34/449 were deleted. Analysis of these cultures during differentiation showed the P-bodies revealed by human index serum and DCP1A-labeled granules in miR-34/449 null MCC cells. By contrast, the apical granules present in the control MCCs were largely undetectable in miR-34/449 null MCC (**Fig. 3d-e**). Given the high abundance of miR-34/449 in MCC (~70% of all miRNAs)[28], this strongly suggests that miR-34/449 is a key cellular component required for the formation of apical granules. The failure to form these granules is likely linked to events that lead to the organization of the apical domain of differentiating MCCs to initiate multicilia formation.

Newly-synthesized proteins are highly concentrated within or adjacent to TNRC6A-containing apical granules

Our study identified TNRC6A concentrated in apical granules lacking enzymes for mRNA decay in MCCs, and showed that TNRC6A is locally required for miRNA target stabilization. These findings led us to speculate that TNRC6A could be involved in mRNA localization and local translation at the apical domain of MCCs. Puromycin was reported to label newly-synthesized proteins, since it mimics aminoacyl-tRNA and can enter the ribosome A site to terminate translation by ribosome-catalyzed covalent incorporation into the nascent polypeptide C-terminus[30]. O-propargyl-puromycin (OPP), an alkyne analog of puromycin, has been used to detect localized translation[30,31]. To visualize newly-synthesized polypeptides in differentiating MCCs, cultures were labeled with OPP for 30min before termination and analyzed at ALI Day 4. OPP staining revealed newly-synthesized proteins strongly localized in apical foci underneath emerging cilia of immature MCCs. Quantitative analysis showed OPP foci ranging from 300-2000nm in diameter and OPP signal intensity about 2.7 folds higher than in their neighboring area ($P<0.0001$)(**Fig. 4a**). The drastic variation in size of these OPP foci, suggested

heterogeneous regulation of protein synthesis in the vicinity of such granules. The similar distribution of OPP foci in differentiating human MCCs from ALI airway epithelial cultures supported the idea of an evolutionary conserved biological process (**Fig. 4b**).

The appearance of OPP foci was cell type-specific and dynamic, as they were not detected in mature MCCs or in other airway epithelial cell types (**Fig. 4a**). OPP signals were abolished by pretreatment with cycloheximide (**Fig. 4c**), supporting the specificity of this approach. The proximity of the OPP foci to apically-located ciliary structures suggested an association with subcellular components implicated in multicilia formation [32,33]. Co-immunostaining of OPP with markers of these structures in ALI day3-4 cultures revealed co-localization with PCM1 and DEUP1, markers of fibrous granules (~800-2000nm in diameter) and deuterosomes (~400-800nm in diameter), respectively. OPP foci were also found abutting centrioles (300-400nm in diameter), marked by Centrin3 antibody (**Fig. 4d-g**). Moreover, co-staining of OPP with human index serum (18033) and DCP1A showed overlap of OPP with apical TNRC6A granules but not with the DCP1A positive P-bodies within the same MCC **(Fig. 5a-b**). In immature MCCs, the TNRC6A granules were also positive for the centriolar protein CCP110, which marks procentrioles. CCP110 signals were found surrounding OPP/DEUP1 double positive foci, suggesting the co-localization of TNRC6A positive granules with procentrioles surrounding deuterosome (**Fig. 5c-e**).

The spatial relationship of TNRC6A granules with centriole biogenesis components was further confirmed by Co-IF staining of human index serum with Centrin 3 or γ-tubulin positive centrioles (**Supplementary Fig. 8a-b**). Co-staining with PCM1 or DEUP1 showed TNRC6A granules immediately above the pericentriolar material and surrounding deuterosomes (**Supplementary Fig. 8c-d**). Altogether the data strongly suggested a connection between TNRC6A granules and the process of centriole amplification.

Components of the translation machinery are concentrated in or adjacent to OPP positive foci.

Having demonstrated the OPP-TNRC6A association, we then asked whether components of the translation machinery were present in the apical OPP-enriched foci. We performed single-molecule fluorescence in situ hybridization (smFISH) for 18S rRNAs, 28s rRNA, MLS mRNA (RNA transcribed from the mitochondrial L-strand DNA) and ribosomal protein 3 (*Rpl3*) mRNA and co-stained with OPP in differentiating ALI day 4 cultures[31].

Confocal analysis revealed minimal to no overlap between 18S, 28S rRNAs with OPP and showed signals largely surrounding OPP positive foci **(Fig. 6a, b, d, f)**. Notably, MLS mRNA, which is abundantly expressed in differentiating MCCs, was not co-localized or associated with OPP foci (**Fig. 6d, f**). By contrast, *Rpl3* mRNA was very enriched in OPP foci, particularly in the smaller more homogeneous population of granules characteristic of the apical TNRC6A-containing granules.

Co-immunostaining of OPP with the translation initiation factors phosphorylated RPS6 (p-RPS6) or eIF3B also showed strong signals double-labeled with OPP in the smaller apical granules (**Supplementary Fig. 9c-d**). By contrast, outside these areas, p-RPS6 and eIF3B expression was found mostly in a non-overlapping pattern around OPP foci (**Supplementary Fig. 9a-b**). Together these findings showed that components of the translation machinery are concentrated either surrounding or in OPP foci associated with TNRC6A apical granules.

Disruption of *Tnrc6a* expression leads to reduced CCP110, abnormal centriologenesis and defective multicilia formation.

We then investigated whether *Tnrc6a* expression was required for the formation of the apical granules in differentiating MCCs. For this, we examined ALI airway epithelial cultures from a *Tnrc6a* null line also carrying an EGFP reporter to identify cells committed to MCC fate (*Tnrc6a^{null}; FOXJ1-EGFP*, see Methods). IF staining of ALI day 4 with human index serum showed that disruption of *Tnrc6a* specifically abolished the apically-localized granules, but not the cytoplasmic P-bodies in FOXJ1-EGFP-labeled multiciliated cells **(Fig. 7a).** We asked how this could affect production of CCP110, a key centriolar protein involved in ciliogenesis and known target of miR-34/449[23]. Thus, we co-cultured airway progenitors from wild type and *Tnrc6a^{null}; FOXJ1-EGFP* mutants and differentiated these cells in ALI cultures. This allowed to compare potential differences in the intensity of signals between *Tnrc6a*-deficient and -sufficient cells side by side, using the latter as internal controls. IF analysis of CCP110 showed strong signals in WT cells but expression was drastically reduced in the *Tnrc6a^{null}; FOXJ1-EGFP* MCCs **(Fig. 7b)**. The presence of FOXJ1-EGFP in *Tnrc6a* mutant cells, suggested no significant defect in MCC fate determination (**Fig. 8a-b**). This was further supported by analysis of E18.5 lungs showing that the proportion of FOXJ1 positive cells in WT and *Tnrc6a^{null}* mutants was essentially the same (**Supplementary Fig. 12)**.

IF staining of these co-cultures of *Tnrc6a^{null}; FOXJ1-EGFP* and WT cells revealed marked differences in levels and distribution of several proteins involved in centriole amplification. For example, in *Tnrc6a* null cells signals for CEP135 and PCM1 were restricted to a single cluster in a corner of the differentiating MCC, characteristic of an early stage of centriole amplification (**Fig. 8a-b**)[34,35]. Moreover, in mutant MCCs PCM1 was found in large cytoplasmic structures indicative of immature centriologenesis and Centrin3 staining was drastically reduced (**Fig. 8b-d**). These changes were compatible with a significant defect of *Tnrc6a* mutant cells in generating the large number of normal centrioles/basal bodies required for multiciliogenesis.

Consistent with a defect in centriologenesis, few cilia formed in MMCs of *Tnrc6a* mutants **(Supplementary Fig. 11a)**. The defect in multicilia formation was further confirmed by examining the trachea of *Tnrc6a* null mutants at E18.5**(Supplementary Fig. 11b-d)**. No gross abnormalities were observed in these embryos or in the overall morphology of their lungs and no compensatory increased expression of other *Tnrc6* family member (*Tnrc6b* and *Tnrc6c*) was observed in Tnrc6A null lungs (**Supplementary Fig. 10**)[18]. Efficient disruption of *Tnrc6a* was demonstrated by IF staining with the monoclonal antibody (4B6), which showed TNRC6A positive granules in tracheal MCCs of wild type but not of mutants (**Supplementary Fig. 11b)**. Co-staining with Ac-α-tub and TNRC6A demonstrated a significantly reduced multicilia staining in *Tnrc6a* null tracheas. Scanning electron microscopy of tracheae from *mutants* showed the majority of MCCs (83%) with shorter and sparser cilia as compared to WT (**Supplementary Fig. 11**, upper panel, n=3, $p<0.01$**)**. While the cilia truncation we found is consistent with an immature MCC phenotype of the *Tnrc6a* null mice, the precise mechanism involved in this shortening is still unclear and will be subject of future studies. However, we found no difference in FOXJ1 staining between WT and *Tnrc6a* null lungs (**Supplementary Fig. 12**), suggesting no defect in MCC fate determination. Transcriptome analysis of WT and *Tnrc6a* null lungs did not detect significant changes in expression of genes associated with proliferation or differentiation of other cell types of the lung. Together, these data strongly support that idea that loss of *Tnrc6a* leads to a defect selectively in MCCs, the same cell type where we found *Tnrc6a* highly expressed in WT lungs.

Discussion

We have previously reported a key role for *Tnrc6a* in the development of the yolk sac endoderm, where it plays a typical function in the miRNA pathway in promoting degradation of miRNA targets[18]. Here we identified expression of *Tnrc6a* selectively present in MCCs of lungs *in vivo* where it is concentrated in a novel class of apically-localized granules containing AGO2, and presumably miRNAs and their targets, adjacent to immature centrioles. Although present in adult airways, these granules are mostly abundant in differentiating immature MCCs. Remarkably, components required for mRNA degradation are missing in these granules, while present in P-bodies within the same MCCs. Instead, they are enriched in components of the mRNA translation machinery and show evidence of concentrated newly-synthesized proteins. We found that, in the lung, loss of *Tnrc6a* leads to broad reduction instead of accumulation of miRNA targets, suggesting a role in target mRNA stabilization, rather than in degradation. This resulted in a drastic reduction of expression of centriolar proteins, known miRNA targets, abnormal centriologenesis and, ultimately, defective MCCs.

Cytoplasmic RNP granules in mammalian cells, including P-body, stress granule, neuronal transport granule and germ granule are generally linked to translation repression. mRNAs are not translated in stress granules where translation initiation factors are concentrated. Indeed, we found no evidence of newly-synthesized polypeptides in P-bodies within the differentiating MCCs. Instead, OPP and translational machinery components were present in the apical TNRC6A-containing granules, suggesting that these are sites of active translation (**Fig. 5**). Our findings, together with reports of active translation associated with FUS granules [36,37], point to a more prevalent role of cytoplasmic RNP granules in active local translation than previously suspected.

Recruitment of TNRC6A to AGO2/miRNA complex triggers typically a cascade of events for translation suppression and target mRNA degradation. This is consistent with reported observations in cultured cells and with our previous report in yolk sac endodermal cells [18,22,38]. However, in addition to recruiting deadenylation complexes to trigger mRNA degradation, TNRC6A can also interact with poly (A) binding proteins (PABP)[39,40] to promote local translation. AGO2 mainly functions as a miRNA binding protein to trigger miRNA-mediated mRNA degradation[41,42]. Interestingly, AGO2 was originally purified and cloned as a translation initiation factor and named EIF2C2[27]. It is known that AGO2 can interact with EIF1A in the biogenesis of miRNAs[43]. miRNAs are well known as a negative regulators of gene expression. However, miRNAs have been also shown to stimulate mitochondrial translation to activate translation of miRNA targets in quiescent cells and to enhance translation initiation mediated by HCV-like IRESes[44-46]

Recent studies have reported TNRC6A or AGO2 localized adjacent to the basal body of primary cilia or centrosomes[47,48], suggesting that the spatial relationship between TNRC6A/AGO2 positive granules and centrioles is conserved in both primary cilia and multicilia (as we report here). We found newly-synthesized proteins (OPP) also concentrated in granules at the base of primary cilia (**Fig. 9**). However, primary cilia remained intact in cultured *Tnrc6a* null cells in contrast to our findings in multicilia. Our data are consistent with the idea that miRNA pathway components, here Tnr6a/AGO and miRNAs, such as miR-34/449 in apical granules might recruit proteins, such as PABP, EIFs and target mRNAs for stabilization and efficient local translation for centriole amplification in differentiating MCCs. Interestingly, proximity-dependent biotinylation (BioID) assays have been previously conducted using dozens of centriolar and cilia proteins as baits to characterize the centrosome-cilium interface[49]. Indeed, these showed TNRC6 family members and AGO family members in close proximity to CEP135

and CEP152. Consistent with our findings, the majority of enzymes involved in mRNA degradation were not associated with centriolar proteins.

In summary, our findings suggest that components of the miRNA pathways in airway MCCs can be organized into specific hubs for target mRNA localization, stabilization and local translation. These observations further provide strong evidence of the critical role of mRNA localization and local translation in organelle biogenesis, as previously proposed based on the prevalence and localization of mRNAs in association with organelles[3].

Acknowledgments: We thank Jun Qian for technical assistance; Dr. Andreas Moor and Dr. Shalev Itzkovitz from the Department of Molecular Cell Biology at Weizmann Institute of Science, Israel, for sharing with us probes for smFISH. We also thank the Lu and Cardoso lab members for thoughtful discussions and input. This study is supported by grants from NHLBI (R01 HL131422 to J.L and W.V.C and R35-HL135834-01 to W.V.C).

Materials and Methods

Mouse breeding, genotyping and monitoring

Tnrc6a$^{gt/gt}$ mutant mice were generated on a mixed genetic background as described[18], and were subsequently backcrossed to C57BL/6 for at least ten generations. Mice are housed in a non-barrier animal facility at Columbia University Medical Center. The genotyping is performed as reported[18]. miR-34/449 null mice were bred and genotyped as described[23]. Foxj1/EGFP/Tnrc6A mice were generated by breeding Tnrc6A^{gt}/+ mice to Foxj1-EGFP mice (Jax, B6; C3-Tg (Foxj1-EGFP)85Leo/J)[50]. All animal studies are carried out with the approval of the Institutional Animal Care and Use Committee (IACUC), Columbia University Medical Campus.

Cloning and packaging of lentiviral vectors

pHAGE-EGFP-Tnrc6a vector was cloned by replacing EGFP fragment of pHAGE-CMV-eGFP-W1 vector (generous gift from Dr. Darrel Kotton, Boston University Medical School) with EGFP-Tnrc6a DNA fragment from pT7-EGFP-Tnrc6A (Addgene #25035) plasmid. To do this, we first cut pHAGE-CMV-EGFP-W1 with NotI (NEB # R0189S), followed by the treatment with DNA Polymerase I, Klenow Fragment (NEB # M0210S) to blunt the end. Then EGFP fragment was released by cutting with BamHI (NEB # R0136S), followed by separation and purification of vector fragment for ligation. To prepare EGFP-Tnrc6a fragment, P7-EGFP-Tnrc6a was cut with AgeII (NEB # R0552S), followed by the treatment with DNA Polymerase I, Klenow Fragment (NEB # M0210S) to blunt the end. Then cut again with BamHI to release and purify EGFP-Tnrc6A fragment. DNA sequencing was performed following ligation and transformation to identify and confirm the right clone. Similarly, EGFP-Ago2 fragment was released from EGFP-Ago2 plasmid (EGFP-C1 backbone, addgene, # 21981) by AgeI, blunted and followed by BamH1 digestion. The same fragment of lentiviral vector used in pHAGE-EGFP-Tnrc6A cloning was used for the ligation to generate pHAGE-EGFP-Ago2.

Packaging of all lentiviral vectors was performed by co-transfection of 293T cells (80% confluent, 15 cm plate) with 2ml of Trans-IT/DNA/media mix containing 5 plasmids encoding the lentiviral backbone (24ug) as well as tat (1.2ug), rev (1.2ug), gag/pol (1.2ug) and vsv-g (2.4ug) viral genes together with 90µl of Trans-IT (MIR #6600). Viral particles in the resulting supernatants were collected 48hrs after transfection and concentrated by ultracentrifugation (90 minutes at 48960g on Beckman SW28 rotor). Titers used in all experiments range from 0.5-1.5 x 10^9TU/ml. For the constructs above, lentiviral infection of basal cells isolated from mouse trachea was performed at the time of seeding and the culture were terminated at Day 3 of the differentiation, when the centriolegensis and ciliogenesis are highly active.

Histological analyses

Tissues were dissected and fixed overnight in in 4% paraformaldahyde (Ted Pella, #18505) overnight at 4°C, then processed either for frozen section or paraffin section by following standard procedures. All the blocks were sectioned at 10 µm either for immunostaining or for in situ hybridization.

β-galactosidase staining

This was performed according to protocol described previously[18]. Briefly, adult lungs of Tnrc6A$^{gt/+}$ mouse were perfused intratracheally with 0.25% glutaraldehyde (Electron Microscopy Science, #16220) at a constant pressure of 30cm H_2O for 30min, then perfused with 1XPBS for 2 hours, followed with staining buffer (5µm C6N6FeK3, 5µm C6N6FeK4, 2mM MgCl2, 1mg/ml X-gal in 1XPBS) for 30min. Then the trachea was tied and the whole lungs were incubated in the staining buffer in a 50ml tube overnight at 37°C. After washing in 1XPBS three times

(2hours for each wash), lungs were fixed again using 4% PFA (Ted Pella, #18505) for 2 hours and then processed for embedding following standard procedures. Sections of LacZ-stained lungs were either subjected to H&E staining or co-stained with antibodies specific for MCCs.

In situ hybridization (ISH)

ISH detection of miR-34a and miR-449a and miR-92b or *Tnrc6a* mRNA expression was performed on frozen sections of mouse lungs using 5' digoxigenin-labeled LNA probes (Exiqon) or digoxigenin-labeled antisense probe of *Tnrc6a*. Briefly, slides were washed with DEPC-treated 1X PBS 3 times for 3 minutes each, followed by the treatment with 100mM triethanolamine buffer (Sigma, Cat #90279) plus 0.25% of acetic anhydride (Sigma, #320102) for 10 minutes, then permeabilized by incubating in PBST (1X PBS plus 0.1% Triton X-100 (Sigma, #9002-93-1) in DEPC-treated water for 30 minutes, and washed 3 times for 5 minutes each at RT in 1X PBS. After 2 hours pre-hybridization using hybridization buffer without labeled probe (50% formamide (American Bioalnalytical, # 95-12-7), 10mM Tris-HCl pH8.0, 600mM NaCl, 1X Denhardt's solution (Sigma, #02532), 200µg/mL tRNA, 1mM EDTA, 0.25% SDS (Ambion, #AM9823), 10% dextran sulfate (American Bioalnalytical, # ab427), hybridizations were carried out at 55°C overnight in the hybridization buffer containing 25nM of DIG-labeled miR-34a (#38487-01, ACAACCAGCTAAGACACTGCCA) or miR-449a (Exiqon, #38587-15, ACCAGCTAACAATACACTGCCA) or miR-92b (Exiqon, #610819-340, CTGCACCGCGTCCCGTC). Then, slides were sequentially washed with SSC (2X, 1X, 0.2X) at 50°C for 30 min. followed by 0.2X SSC (Ambion, #AM9763) for 5 minutes at RT, and finally 1X PBS for 5 minutes at RT. Slides were then incubated in blocking solution (TTBS, 0.05M Tris, pH 7.5, 0.15M NaCl, 0.1% Tween-20, plus 5% sheep serum) and incubated with anti-digoxigenin-AP, Fab fragments (1:500, Roche, Cat. #11093274910) overnight at 4°C. After washing in TTBS 3 times for 10 minutes each, signals were developed using BM purple (Roche, # 11442074001). Hybridization for Tnrc6A using digoxigenin-labeled antisense probe was performed at 70°C by following the standard procedure. ISH of Spef2 and Rsph1 was performed by RNAscope according to manufacture's protocol.

Immunofluorescence (IF) and immunohistochemistry (IHC)

For IHC, paraffin sections were deparaffinized and rehydrated by sequentially incubating sections in three washes of xylene (5 min each), two washes of 100% ethanol (10 min each), two washes of 95% ethanol (10 min each), followed by two washes in dH_2O (5 min each). Endogenous peroxidase was quenched by incubation with 0.3% H_2O_2/0.3% horse serum in 1X PBS for 5 minutes at RT. Then, slides were washed in TNT buffer (0.1M Tris pH 7.5, 0.15M NaCl, 0.05% Tween-20) 3 times (5min each), followed by blocking with TNB buffer (0.1M Tris pH 7.5, 0.15M NaCl, 0.5% blocking reagent) for one hour at RT. Incubation with Ac-α-tub antibody (Sigma, #T7451, 1:10,000) diluted in TNB buffer overnight at 4°C. Slides were then washed with TNT buffer 3 times, incubated with Horseradish peroxidase (HRP) conjugated secondary antibodies (Life Technologies) for 2 hours at RT, signals were developed by using the DAB staining kit (Vector Laboratories, Cat.# SK-4100).

When TNRC6A monoclonal antibody (Santa Cruz, 4B6, # sc-56314) was used for immunohistochemistry, TSA Plus Fluorescence Kit (Perkin Elmer, # NEL741B001KT) was used for signal amplification. After incubating with HRP-conjugated secondary antibody, signals of slides or ALi filters were developed by TSA Plus Working Solution following manufacture's protocol.

For IF staining, cryosections or transwell filter of ALI cultures were washed in PBS, and then blocked by 5% donkey serum in PBST (1XPBS, 0.3% Triton X-100) for one hour at RT, followed by incubation with primary antibodies overnight at 4°C (TNRC6A, human index serum, 1:3000;

FOXJ1, eBioscience, # 14-9965-82, 1:100; Ac-α-tub, Sigma, # T7451, 1:10,000, or Abcam # ab125356; DCP1A, Abcam, #ab183709, 1:50; DDX6, Cell Signaling Technology, #8988S, 1:20; EDC3, Santa Cruz, # sc-55081, 1:20; EDC4/GE-1, Cell Signaling Technology, #2548S, 1:50; Xrn1, Bethyl Laboratories, #A300-443A, 1:20; γ-tubulin, Abcam, #ab84355, 1:50; EIF3B, Santa Cruz , # sc-16377, 1:50). DEUP1, Dr Xueliang Zhu's lab, 1:300; PCM1, Cell Signaling, #5213, 1:50. Alexa Fluor 488 or 568-conjugated secondary antibodies (Donkey anti-Mouse IgG, or Donkey anti-Rabbit IgG or Donkey anti-Goat IgG; Life Technologies, 1:250 dilution) and Alexa Fluor 594 phalloidin (Life Technologies, #A22287) were used for the visualization of signals. Zeiss 710 confocal microscope was used for the image acquisition and analysis.

Single-molecule fluorescence in situ hybridization (smFISH)

ALI cultured filters are fixed for 15 min in 4% PFA, followed by three washed in PBS then transfer to 70% ethanol for storage. In situ hybridization and imaging were performed as previously reported[51]. Fluorescence labeled DNA oligo probes are from Itzkovitz's Laboratory. All probes are labeled with Cy5 except rRNA 18s (TMR).

O-Propargyl-puromycin (OPP) labeling and imaging

ALI cultures were treated with either 50µg/ml Cycloheximide (Sigma-Aldrich, C7698) or DMSO control for 15 min, followed by 30 min incubation with 50µM OPP (Jena Bioscience, NU-913-5). Cultures were then washed with room temperature PBS and fixed with 4 % of PFA, followed by three washes in PBS. OPP features an alkyne group that can be detected and imaged by the addition of azide-coupled fluorophores in the highly specific click reaction[30]. The click reaction was performed subsequently to the IF staining by making use of the Click-iT Alexa Fluor 488 or Click-iT Alexa Fluor 647 Imaging Kits (Thermo Fisher Scientific, C10337 and C10340). The kits were used according to the manufacturer's instruction with the exception of an additional 20-fold dilution of the working solution of the Alexa Fluor azide dye in DMSO.

Differentiation of MCCs in an Air-Liquid Interface (ALI) of trachea progenitors

Primary tracheal progenitor were cultured and differentiated as described previously[21]. Briefly, tracheas from adult (8- to 12-weeks old, C57BL/6) mice were dissected and cleaned in ice-cold Ham's F-12 medium (Life Technologies, #31765-092) with 1% penicillin/streptomycin (Life Technologies, # 15140-163). To isolate epithelial cells, tracheas were digested in 1.5mg/ml Pronase (Roche, #10165921001) in Ham's F-12 media overnight at 4°C. The digestion was stopped by fetal bovine serum (FBS, sigma, #12133C, a final concentration of 10%). The epithelial cells including basal cells were dislodged from trachea by gentle inverting the tube, and medium containing epithelial cells was transferred to another tube. This was repeated for three time and medium containing epithelial cells were pooled and Centrifuge at 500Xg, 4°C, for 10 min. After removing the medium, epithelial cells were treated with DNase (200µl per trachea) on ice for 5min, and spin down again at 500Xg, 4°C. The pelleted cells were washed by pre-warmed mTEC/Basic medium containing advanced DMEM/F-12 (Life Technologies, #12634-028), 15mM HEPES (Life Technologies, #15630-080), 1% penicillin/streptomycin, 4mM glutamine (Life Technologies, #35050-061), 3.6mM sodium bicarbonate (Life Technologies, #25080-094), and 0.25ug/mL Amphotericin B (Life Technologies, #15290-018), and centrifuged at 500 × g for 5 min. Then cells were resuspended in mTEC/Plus medium, which contained mTEC/Basic medium with 5% FBS, 25ng/ml Epidermal Growth factor (EGF) (Corning, #354001), 10µg/ml Insulin (Sigma, #I6634), 5 µg/ml Transferrin (Sigma, #T1147), 0.1 µg/ml Cholera Toxin (Sigma, #C8052), 30 µg/ml Bovine Pituitary Extract (BPE)(sigma,#P1476), and freshly added 50nM retinoic acid (RA, Sigma, #R2625), and plated on rat tail type I collagen (Advanced Biomatrix, #5056) coated trans-wells (Corning, #3470) of 24-well plates. 10uM Rock inhibitor Y27632 (Tocris, # 1254) was added to mTEC/Plus only once when the cells were plated. The mTEC/Plus medium was changed every other day for 7 days, until we switched the culture to

air-liquid interface culture by removing the media in the apical chamber, and replacing the media in the basal chamber with mTEC/SF medium. The mTEC/SF medium was changed every other day until the culture was terminated at different time point. Cultures were terminated at different time point after the induction of differentiation and harvested for RNA isolation or Immunofluorescence. For IF, cultures filters were washed with room temperature PBS twice, then fixed by 4% PFA for 15min, followed by three time of washes in PBS, and keep them in PBS at 4°C.

Scanning Electron Microscopy (SEM)

Trachea of E18.5 WT or Tnrc6A$^{gt/gt}$ embryonic lungs were dissected and cleaned in PBS. Trachea were quickly transferred to a vial contain fresh prepare 2.5% glutaraldehyde, 0.1 M sodium Cacodylate, 0.2 M Sucrose, 5mM MgCl2 pH 7.4. Dehydrate through a graded series of ethanol. Critical point dry using liquid carbon dioxide in a Tousimis Samdri 795 Critical Point Drier (Rockville MD). Sputter coat with chromium in a Quorum EMS 150T ES (Quorum Technologies Ltd, United Kingdom). Examine in a Zeiss Supra Field Emission Scanning Electron Microscope (Carl Zeiss Microscopy, LLC North America), using an accelerating voltage of 2 KV. N=2, and about 120 cells were counted for each sample.

IF signal quantitation and Statistical analysis

To quantify the IF staining of newly synthesized proteins (OPP) and other centriolar proteins. Z-stack of confocal images were taken for the entire cells. For OPP staining, several planes that cover the entire positive foci will be chosen and perform maximal project for these planes. Then the area of foci and background were marked by ImageJ followed by the calculation of mean optical intensity. For other centriolar proteins, we first generate maximal projection image for entire cells, and drew the cell boundaries. Then the mean optical intensities were measured by ImageJ. Data are presented as the mean ± SEM were subjected to 2-tailed, paired Student's t test. $P < 0.05$ was considered significant. In all experiments a minimum of 3-4 replicates (ALI cultures or lung sections) were used for analyses.

Data availability

Data referenced in this study are available in the National Center for Biotechnology Information Gene Expression Omnibus (GEO) and are accessible through the GEO Series accession number GSE89327, GSE30244 and GSE89327. The data is available in link https://drive.google.com/drive/folders/15JZ_G_kxdZSpjS9dw1tIHfZEds-dUNwk?usp=sharin. All other relevant data are available from the corresponding author on request.

References

1 Joshi, A. S., Zhang, H. & Prinz, W. A. Organelle biogenesis in the endoplasmic reticulum. *Nat Cell Biol* **19**, 876-882, doi:10.1038/ncb3579 (2017).

2 Nunnari, J. & Walter, P. Regulation of organelle biogenesis. *Cell* **84**, 389-394 (1996).

3 Lecuyer, E. *et al.* Global analysis of mRNA localization reveals a prominent role in organizing cellular architecture and function. *Cell* **131**, 174-187, doi:10.1016/j.cell.2007.08.003 (2007).

4 Weis, B. L., Schleiff, E. & Zerges, W. Protein targeting to subcellular organelles via MRNA localization. *Biochim Biophys Acta* **1833**, 260-273 (2013).

5 Cui, X. A. & Palazzo, A. F. Localization of mRNAs to the endoplasmic reticulum. *Wiley Interdiscip Rev RNA* **5**, 481-492, doi:10.1002/wrna.1225 (2014).

6 Vertii, A., Hehnly, H. & Doxsey, S. The Centrosome, a Multitalented Renaissance Organelle. *Cold Spring Harb Perspect Biol* **8**, doi:10.1101/cshperspect.a025049 (2016).

7 Yan, X., Zhao, H. & Zhu, X. Production of Basal Bodies in bulk for dense multicilia formation. *F1000Res* **5**, doi:10.12688/f1000research.8469.1 (2016).

8 Sepulveda, G. *et al.* Co-translational protein targeting facilitates centrosomal recruitment of PCNT during centrosome maturation in vertebrates. *Elife* **7**, doi:10.7554/eLife.34959 (2018).
9 Alliegro, M. C., Alliegro, M. A. & Palazzo, R. E. Centrosome-associated RNA in surf clam oocytes. *Proc Natl Acad Sci U S A* **103**, 9034-9038, doi:10.1073/pnas.0602859103 (2006).
10 Iaconis, D. *et al.* The centrosomal OFD1 protein interacts with the translation machinery and regulates the synthesis of specific targets. *Sci Rep* **7**, 1224, doi:10.1038/s41598-017-01156-x (2017).
11 Braun, J. E., Huntzinger, E. & Izaurralde, E. The role of GW182 proteins in miRNA-mediated gene silencing. *Adv Exp Med Biol* **768**, 147-163, doi:10.1007/978-1-4614-5107-5_9 (2013).
12 Liu, J. *et al.* A role for the P-body component GW182 in microRNA function. *Nat Cell Biol* **7**, 1261-1266, doi:10.1038/ncb1333 (2005).
13 Cougot, N. *et al.* Dendrites of mammalian neurons contain specialized P-body-like structures that respond to neuronal activation. *J Neurosci* **28**, 13793-13804, doi:10.1523/JNEUROSCI.4155-08.2008 (2008).
14 Huang, Y. W., Ruiz, C. R., Eyler, E. C., Lin, K. & Meffert, M. K. Dual regulation of miRNA biogenesis generates target specificity in neurotrophin-induced protein synthesis. *Cell* **148**, 933-946, doi:10.1016/j.cell.2012.01.036 (2012).
15 Sen, G. L. & Blau, H. M. Argonaute 2/RISC resides in sites of mammalian mRNA decay known as cytoplasmic bodies. *Nat Cell Biol* **7**, 633-636, doi:10.1038/ncb1265 (2005).
16 Nishi, K., Nishi, A., Nagasawa, T. & Ui-Tei, K. Human TNRC6A is an Argonaute-navigator protein for microRNA-mediated gene silencing in the nucleus. *Rna* **19**, 17-35, doi:10.1261/rna.034769.112 (2013).
17 Jain, S. & Parker, R. The discovery and analysis of P Bodies. *Adv Exp Med Biol* **768**, 23-43, doi:10.1007/978-1-4614-5107-5_3 (2013).
18 Jiang, Z. *et al.* Trinucleotide repeat containing 6a (Tnrc6a)-mediated microRNA function is required for development of yolk sac endoderm. *The Journal of biological chemistry* **287**, 5979-5987, doi:10.1074/jbc.M111.297937 (2012).
19 Eystathioy, T. *et al.* A phosphorylated cytoplasmic autoantigen, GW182, associates with a unique population of human mRNAs within novel cytoplasmic speckles. *Mol Biol Cell* **13**, 1338-1351, doi:10.1091/mbc.01-11-0544 (2002).
20 Lian, S. *et al.* GW bodies, microRNAs and the cell cycle. *Cell Cycle* **5**, 242-245, doi:10.4161/cc.5.3.2410 (2006).
21 You, Y. & Brody, S. L. Culture and differentiation of mouse tracheal epithelial cells. *Methods Mol Biol* **945**, 123-143, doi:10.1007/978-1-62703-125-7_9 (2013).
22 Eulalio, A., Helms, S., Fritzsch, C., Fauser, M. & Izaurralde, E. A C-terminal silencing domain in GW182 is essential for miRNA function. *Rna* **15**, 1067-1077, doi:10.1261/rna.1605509 (2009).
23 Song, R. *et al.* miR-34/449 miRNAs are required for motile ciliogenesis by repressing cp110. *Nature* **510**, 115-120, doi:10.1038/nature13413 (2014).
24 Wu, J. *et al.* Two miRNA clusters, miR-34b/c and miR-449, are essential for normal brain development, motile ciliogenesis, and spermatogenesis. *Proc Natl Acad Sci U S A* **111**, E2851-2857, doi:10.1073/pnas.1407777111 (2014).
25 Jakymiw, A. *et al.* Disruption of GW bodies impairs mammalian RNA interference. *Nat Cell Biol* **7**, 1267-1274, doi:10.1038/ncb1334 (2005).
26 Bloch, D. B., Gulick, T., Bloch, K. D. & Yang, W. H. Processing body autoantibodies reconsidered. *Rna* **12**, 707-709, doi:10.1261/ rna.17406 (2006).
27 Meister, G. *et al.* Identification of novel argonaute-associated proteins. *Current biology : CB* **15**, 2149-2155, doi:10.1016/j.cub.2005.10.048 (2005).
28 Marcet, B. *et al.* Control of vertebrate multiciliogenesis by miR-449 through direct repression of the Delta/Notch pathway. *Nat Cell Biol* **13**, 693-699, doi:10.1038/ncb2241 (2011).
29 Wang, L. *et al.* miR-34b regulates multiciliogenesis during organ formation in zebrafish. *Development* **140**, 2755-2764, doi:10.1242/dev.092825 (2013).

30 Liu, J., Xu, Y., Stoleru, D. & Salic, A. Imaging protein synthesis in cells and tissues with an alkyne analog of puromycin. *Proc Natl Acad Sci U S A* **109**, 413-418, doi:10.1073/pnas.1111561108 (2012).
31 Moor, A. E. *et al.* Global mRNA polarization regulates translation efficiency in the intestinal epithelium. *Science* **357**, 1299-1303, doi:10.1126/science.aan2399 (2017).
32 Mori, M. *et al.* Cytoplasmic E2f4 forms organizing centres for initiation of centriole amplification during multiciliogenesis. *Nat Commun* **8**, 15857, doi:10.1038/ncomms15857 (2017).
33 Zhao, H. *et al.* The Cep63 paralogue Deup1 enables massive de novo centriole biogenesis for vertebrate multiciliogenesis. *Nat Cell Biol* **15**, 1434-1444, doi:10.1038/ncb2880 (2013).
34 Vladar, E. K. & Stearns, T. Molecular characterization of centriole assembly in ciliated epithelial cells. *J Cell Biol* **178**, 31-42, doi:10.1083/jcb.200703064 (2007).
35 Kubo, A., Sasaki, H., Yuba-Kubo, A., Tsukita, S. & Shiina, N. Centriolar satellites: molecular characterization, ATP-dependent movement toward centrioles and possible involvement in ciliogenesis. *J Cell Biol* **147**, 969-980 (1999).
36 Weil, T. T. *et al.* Drosophila patterning is established by differential association of mRNAs with P bodies. *Nat Cell Biol* **14**, 1305-1313, doi:10.1038/ncb2627 (2012).
37 Yasuda, K. *et al.* The RNA-binding protein Fus directs translation of localized mRNAs in APC-RNP granules. *J Cell Biol* **203**, 737-746, doi:10.1083/jcb.201306058 (2013).
38 Eulalio, A., Huntzinger, E. & Izaurralde, E. GW182 interaction with Argonaute is essential for miRNA-mediated translational repression and mRNA decay. *Nature structural & molecular biology* **15**, 346-353, doi:10.1038/nsmb.1405 (2008).
39 Huntzinger, E., Braun, J. E., Heimstadt, S., Zekri, L. & Izaurralde, E. Two PABPC1-binding sites in GW182 proteins promote miRNA-mediated gene silencing. *EMBO J* **29**, 4146-4160, doi:10.1038/emboj.2010.274 (2010).
40 Tritschler, F., Huntzinger, E. & Izaurralde, E. Role of GW182 proteins and PABPC1 in the miRNA pathway: a sense of deja vu. *Nat Rev Mol Cell Biol* **11**, 379-384, doi:10.1038/nrm2885 (2010).
41 Peters, L. & Meister, G. Argonaute proteins: mediators of RNA silencing. *Mol Cell* **26**, 611-623, doi:10.1016/j.molcel.2007.05.001 (2007).
42 Meister, G. *et al.* Human Argonaute2 mediates RNA cleavage targeted by miRNAs and siRNAs. *Mol Cell* **15**, 185-197, doi:10.1016/j.molcel.2004.07.007 (2004).
43 Yi, T. *et al.* eIF1A augments Ago2-mediated Dicer-independent miRNA biogenesis and RNA interference. *Nature Communications* **6**, 7194, doi:10.1038/ncomms8194 (2015).
44 Zhang, X. *et al.* MicroRNA directly enhances mitochondrial translation during muscle differentiation. *Cell* **158**, 607-619, doi:10.1016/j.cell.2014.05.047 (2014).
45 Bukhari, S. I. A. *et al.* A Specialized Mechanism of Translation Mediated by FXR1a-Associated MicroRNP in Cellular Quiescence. *Mol Cell* **61**, 760-773, doi:10.1016/j.molcel.2016.02.013 (2016).
46 Mengardi, C. *et al.* microRNAs stimulate translation initiation mediated by HCV-like IRESes. *Nucleic Acids Res* **45**, 4810-4824, doi:10.1093/nar/gkw1345 (2017).
47 Moser, J. J., Fritzler, M. J. & Rattner, J. B. Repression of GW/P body components and the RNAi microprocessor impacts primary ciliogenesis in human astrocytes. *BMC Cell Biol* **12**, 37, doi:10.1186/1471-2121-12-37 (2011).
48 Aizer, A. *et al.* The dynamics of mammalian P body transport, assembly, and disassembly in vivo. *Mol Biol Cell* **19**, 4154-4166, doi:10.1091/mbc.E08-05-0513 (2008).
49 Gupta, G. D. *et al.* A Dynamic Protein Interaction Landscape of the Human Centrosome-Cilium Interface. *Cell* **163**, 1484-1499, doi:10.1016/j.cell.2015.10.065 (2015).
50 Ostrowski, L. E., Hutchins, J. R., Zakel, K. & O'neal, W. K. Targeting expression of a transgene to the airway surface epithelium using a ciliated cell-specific promoter. *Mol Ther* **8**, 637-645 (2003).

51 Moor, A. E. *et al.* Global mRNA polarization regulates translation efficiency in the intestinal epithelium. *Science* **357**, 1299-1303 (2017).

Figure Legends

Fig. 1. *Tnrc6a* is selectively expressed in multiciliated cells (MCCs) of airways in the mouse lungs.

a) β-galactosidase staining (LacZ) of adult lungs of *Tnrc6a*$^{gt/+}$ reporter mice showing selective expression in the airway epithelium (blue arrow), compared to vascular (red arrow) and the alveolar structures.

b) Tnrc6a in situ hybridization confirming expression in airway epithelium (blue arrow), but not in vessels (red arrow) or alveoli (outlined by dashed line).

c) High levels of β-galactosidase signals (blue arrow) in multiciliated cells labeled by Ac-α-tub (brown arrow) compared to other airway cell types.

d) Immunostaining with human index serum (18033: green) detects TNRC6A in MCCs (Ac-α-tub: red).

e) Time course of detection of Tnrc6a-containing cytoplasmic granules in MCCs (FOXJ1+) differentiating from adult airway progenitors in air-liquid interface (ALI) cultures.

f) Co-staining of Ac-α-tub with TNRC6A (human index serum) showing TNRC6A positive granules more abundant in immature MCCs (outlined by dashed lines) with much less Ac-α-tub (red) signals than in mature MCCs.

Fig. 2. TNRC6A protein concentrates in apically-localized granules that lack mRNA degradation enzymes (a-i: immunofluorescence, ALI airway epithelial cultures).

a-b) TNRC6A monoclonal antibody (clone#:4B6) detects a novel class of apically-localized granules (highlighted by dashed lines) underneath the multicilia (red, Ac-α-tub). X-Z projection of confocal z-stack images (white: DAPI nuclei).

c) Apically-localized granules detected by human index serum (18033). Dashed lines depict a plane of Z-stack image from the apical area of a MCC.

d) Randomly-localized granules (P-bodies) detected by human index serum. Dashed lines depict a plane of Z-stack image of the same MCC in panel (c) at the level of nuclei (red: FOXJ1; white, DAPI).

e) 3D view of Z-stack images and diagram of a single MCC showing apical (red dashed box) and randomly-localized (P-bodies) granules.

f) Co-staining of EDC4 with human index serum in a single MCC. EDC4 mainly present in P-bodies instead of apical granules (dashed box).

g) TNRC6A-EGFP fusion protein expressed by a lentiviral vector concentrates in apical granules of MCC identified by co-labeling with γ-tub (boxed area) in ALI day3 culture.

h-i) Co-staining of DCP1A with human index serum showing DCP1A largely in P-bodies instead of the apical granules (dashed box) in a single MCC. Diagram depicts distinct components of these granules.

Fig. 3. Apically-localized granules contain AGO2 and miRNAs

a) Co-staining of AGO2 (green, clone 11A9) and TNRC6A (red, human index serum) showing double-labeling in both apical granules and P-bodies within the same MCC (diagram). AGO2 protein is also detected in nuclei of MCC.

b) AGO2-EGFP fusion protein produced by a lentiviral vector in MCC differentiated in ALI cultures form apical granules underneath the emerging cilia (red, Ac-α-tub, red arrow point to concentrated AGO2-EGFP fusion protein underneath cilia).

c) In situ hybridization (ISH) showing miR-449a enriched in apical area of MCCs (red arrow) underneath the cilia (red bracket).

d) Co-staining of DCP1A(red) with human index serum (green) in ALI day 4 cultures from control airway progenitors showing abundant apical granules (single-labeled green) and P-bodies (double-labeled yellow) in MCCs. MCCs from miR-34/449 null (miR-34/449 triple KO) cultures showing less apical granules

e) Diagram depicts the distinct components of these granules.

Fig. 4. Newly-synthesized proteins are concentrated in fibrous granules, deuterosomes and apical granules adjacent to centrioles.
a) Newly synthesized proteins labeled with OPP (red) and cilia (green, Ac-α-tub). OPP signal concentrated in apically localized foci of immature mouse MCCs (with shorter and less cilia, white dashed line), but not in mature mouse MCCs (full grown cilia, brown dashed line) and other cell types (red dashed line). The mean optical density of OPP positive foci and neighboring area in total, OPP foci in 30 immature MCCs from three independent cultures were analyzed (Image J software).
b) Similar pattern observed in human immature MCCs.
c) OPP signal abolished by pretreatment of cycloheximide, a protein synthesis inhibitor.
d) Illustration of OPP positive foci in the apical area of both human and mouse immature MCCs.
e-g) OPP foci (red) are present in deuterosomes (marked by DEUP1 staining), or fibrous granules (marked by PCM1) are adjacent or overlapping centrioles (marked by Centrin3). Diagrams depicting the relationship of these components with the small and large OPP foci.
Images in e, f, g: A plane of Z-stack images from the apical area of a single MCC. ***:P<0.0001.

Fig. 5. Newly synthesized proteins are highly concentrated within or adjacent to apically-localized TNRC6A positive granules in ALI day 3 cultures.
a. IF-co-staining of OPP (red, newly-synthesized proteins) with DCP1A (pink) and human index serum (green, 18033) showing OPP concentrated in apical TNRC6A positive granules, but not in DCP1A positive P-bodies of the same MCC. 3D view of Z-stack images of a single MCC.
b. Apical TNRC6A-positive granules (green) overlap or are tightly abutting OPP foci (red, A plane of Z-stack image of the apical region of single MCC). Schematics depicting the TNRC6A-interaction with smaller OPP foci but not with the larger OPP foci (see in c,d).
c, d, e. In some MCCs, TNRC6A positive granules surround OPP foci which is also DEUP1 positive. DCP1A signals do not overlap with TNRC6A or OPP. Deuterosome-associated TNRC6A positive granules co-localize with procentrioles marked by CCP110 staining. A plane of Z-stack image of apical region of single MCC in all images.
f. Schematics of the patterns of expression during centriole amplification. OPP (smaller foci), TNRC6A, DEUP1, CCP110.

Fig. 6. Fig. 6. rRNAs and mRNAs for the ribosomal proteins are associated with OPP positive foci in differentiating MCCs in ALI at Day 3 cultures. RNAs detected by smFISH. A plane of Z-stack image of the apical region of a single MCC shown in each panel. Diagram (right) summarizing findings.
a-b) 18s and 28s rRNA (white arrow head) are found surrounding OPP foci.
c) Top panel: *Rpl3* mRNA is highly concentrated in OPP foci of the smaller more homogeneous apical granules (Tnr6a-containing). Bottom panel: Larger more heterogenous OPP foci also co-label with *Rpl3* but to a smaller extent.
d) RNA transcribed from the mitochondrial L-strand DNA does not overlap with OPP foci.

Fig. 7. Disruption of *Tnrc6a* expression leads to the loss of apical granules and a significant reduction of CCP110 protein.
a) *Tnrc6a* null mutant MCCs are marked by FOXJ1-EGFP (green), human index serum (red) stains both apical granules and P-bodies. However in these mutants apical granules are absent (area outlined by dashed lines) due to loss of Tnr6a.
b) CCP110 protein detected by IF staining of co-cultures of *Tnrc6a* null mutant MCCs (marked by FOXJ1-EGFP, pink, outlined by green dashed line) with WT control cells (outlined by red dashed line). CCP110 is nearly absent in *Tnrc6a* null MCCs.

Fig. 8. Defective centriole amplification in *Tnrc6a* mutant cells.
a, b) CEP135 or PCM1 proteins (red) were detected by IF staining of co-cultures of *Tnrc6a* mutant MCCs (marked by FOXJ1-EGFP, green, outlined by white dashed line) with WT control cells (outlined by green dashed line) differentiating in ALI interface cultures .
c) IF detection of Centrin3 protein (red) in wild type (top panel, dashed lines) and *Tnrc6a* mutant MCCs differentiating in ALI interface cultures (bottom panel, dashed lines, visualized in green by FOXJ1-EGFP expression). Marked decrease in centrin 3 expression in mutant MCCs. The mean optical density of IF signaling (Intensity mean value) was quantified using Image J software. In total, IF staining signal of 30 MCCs from three independent cultures (n=3) were quantified. ***: P<0.0001.

Fig. 9. Disruption of *Tnrc6a* does not prevent primary cilia from forming. IF of ALI airway epithelial cultures at day3
a) WT ALI airway epithelial cultures: newly-synthesized proteins (red, labeled by OPP) are concentrated in foci at the base of primary cilia (green).
b) Co-culture of WT and Tnrc6a null; FOXJ1-EGFP cells a ALI day3 : *Tnrc6a* null cells marked by FOXJ1-EGFP (green) showing no significant defect in primary cilia marked by Ac-α-tub staining (red**).**

Supplementary Information

Supplementary table 1. Genes most downregulated in *Tnrc6a* null lungs

Supplementary Fig. 1. (page 1-2)**.** miRNA targets enriched among the genes upregulated in *Tnrc6a null* yolk sac.

Supplementary Fig. 2. (pages 1-2) miRNA targets enriched among the genes downregulated in E18.5 *Tnrc6a* null lungs.

Supplementary Fig. 3. Levels of miR-449a and miR-146b are not altered in *Tnrc6a*$^{gt/gt}$ lungs.

Supplementary Fig. 4. miR-34/449 targets are downregulated in *Tnrc6a*^{null} lungs
(**a**) qRT-PCR confirmation of gene targets of miR-34/449 downregulated in *Tnrc6a*^{null} lungs initially detected in our transcriptome analysis.
(b) *Spef2* and *Foxj1* dual in situ hybridization (RNAscope) showing strong *Spef2* signals (arrow) in MCCs of WT reduced (*) in MCCs of *Tnrc6a*^{null} (representative large airway from both groups: d, dorsal; v, ventral).
(c) Rsph1-acetylated a-Tubulin double immunofluorescence showing strong Rsph1 signals in WT MCCs (arrow bottom left) reduced in *Tnrc6a*^{null} airways (* bottom right).

Supplementary Fig. 4. miR-34/449 targets are downregulated in Tnrc6a^{null} lungs.
(a) qRT-PCR confirmation of gene targets of miR-34/449 downregulated in *Tnrc6a*^{null} lungs initially detected in our transcriptome analysis (n=3 per group).
(b) *Spef2* and *Foxj1* dual in situ hybridization (ISH, RNAscope) showing strong *Spef2* signals (arrow) in MCCs of WT reduced (*) in MCCs of *Tnrc6a*^{null} (representative large airway from both groups: d, dorsal; v, ventral).
(c) Rsph1-acetylated a-Tubulin double immunofluorescence showing strong Rsph1 signals in WT MCCs (arrow bottom left) reduced in *Tnrc6a*^{null} airways (* bottom right). Right panel:

Double ISH of *Rsph1-Foxj1* confirming strong Rsph1 cytoplasmic signals in WT MCCs decreased in mutant MCCs . (b, c) representative images of n=2 lungs per group. Bars in b, c = 12um and 15 um, respectively.

Supplementary Fig. 6. Apical granules lack enzymes for mRNA degradation.
a) Each panel represents a 3D image of confocal Z-stack images of a single MCC in culture. Apically localized granules are highlighted by dashed lines. TNRC6A stained with human Index serum (18033). DCP1A, DDX6 and XRN1 are concentrated in randomly-localized granules (P-bodies). However, DCP1A and DDX6 are undetectable in apically granules. XRN1 are present in small number of apically granules at low levels.
b) Co-localization profile of apically- localized or randomly- localized granules (P-bodies) within the same MCC indicating the different concentration of these proteins in these two classes of granules. Percentage of granules with double labeling signal.

Supplementary Fig. 7. Apically-enriched ISH signal of miRNAs in multiciliated cells of airways in vivo.
a-b) In situ hybridization of miR-34a and miR-34b. Apically-localized signals (red arrow) underneath multicilia (bracket)

Supplementary Fig. 8. Apical TNRC6A positive granules are adjacent to centrioles. Co-staining of TNRC6A (green or red, human index serum, 18033) with Centrin 3 (red, a), γ-tubulin (red, b), PCM1 (green, c) and DEUP1 (red, d). A plane of Z-stack image of apical region of single MCC is shown in each panel.

Supplementary Fig. 9. Translation initiation factors are closely associated with apical OPP foci. All panels: confocal images of a single MCC in airway ALI culture. Diagram (right) summarizing findings.
a, b) Translation initiation factors (EIF3B and p-RPS6) overlap with OPP in smaller more homogenously-shaped apical granules (expected to contain TNRC6A). Phalloidin stained cell membrane depicts apical region of MCC.
c, d) Immediately below these regions, where large OPP foci were mostly found, EIF3B and p-RPS6 proteins were present in a non-overlapping pattern (high magnification panel shown in the right enlarged from the boxed area).

Supplementary Fig. 10.
a) Disruption of *Tnrc6a* expression in *Tnrc6a* null lungs results in no compensation by *Tnrc6b* and *Tnrc6c* expression.
b) No gross abnormalities were observed in *Tnrc6a* null lungs embryos at E18.5.

Supplementary Fig. 11. Disruption of *Tnrc6a* results in defective multicilia formation.
a) Tnrc6a mutant cells marked by FOXJ1-EGFP (green) and co-cultured with WT control cells fail to form multicilia marked by Ac-α-tub
b) Co-IF staining of TNRC6A (green, monoclonal antibody 4B6) and Ac-α-tub (red) of wild type or *Tnrc6a*$^{gt/gt}$ airways.
c) Scanning electron microscopy of trachea of wild type or *Tnrc6a* null mice (right panels are enlarged images of highlighted areas by dashed lines); defective (red arrow head) and well differentiated (light blue arrow) multiciliated cells in WT and mutant trachea.
d) Percentage of multiciliated cells with short and sparse cilia in WT and *Tnrc6a* null tracheas (n=2, $p<0.01$).

Supplementary Fig. 12. No differences in FOXJ1 expression is detected in wild type or *Tnrc6a null* airways.

a-b) FOXJ1 staining in E18.5 wild type and *Tnrc6a* null airways.

c) Percentage of FOXJ1 positive cells in the airways of wild type and *Tnrc6a* null embryos.

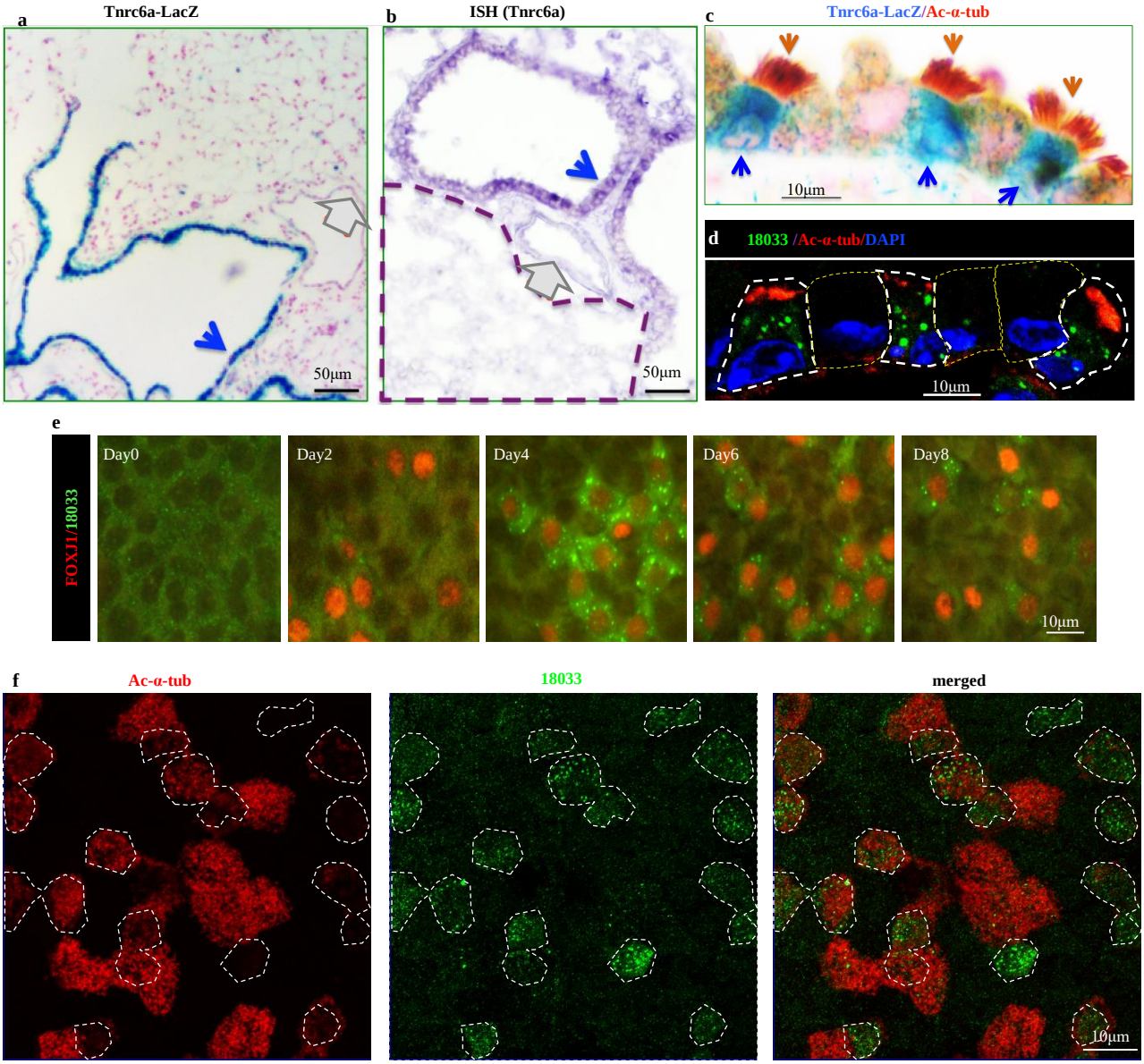

Fig. 1. *Tnrc6a* is selectively expressed in multiciliated cells (MCCs) of airways in the mouse lungs.

a) β-galactosidase staining (LacZ) of adult lungs of *Tnrc6a*$^{gt/+}$ reporter mice showing selective expression in the airway epithelium (blue arrow), compared to vascular (gray arrow) and alveolar structures.

b) Tnrc6a in situ hybridization confirming expression in airway epithelium (blue arrow), but not in vessels (red arrow) or alveoli (outlined by dashed line).

c) High levels of β-galactosidase signals (blue arrow) in multiciliated cells labeled by Ac-α-tub (brown arrow) compared to other airway cell types.

d) Immunostaining with human index serum (18033: green) detects TNRC6A in MCCs (Ac-α-tub: red).

e) Time course of detection of Tnrc6a-containing cytoplasmic granules in MCCs (FOXJ1+) differentiating from adult airway progenitors in air-liquid interface (ALI) cultures.

f) Co-staining of Ac-α-tub with TNRC6A (human index serum) showing TNRC6A positive granules more abundant in immature MCCs (outlined by dashed lines) with much less Ac-α-tub (red) signals than in mature MCCs.

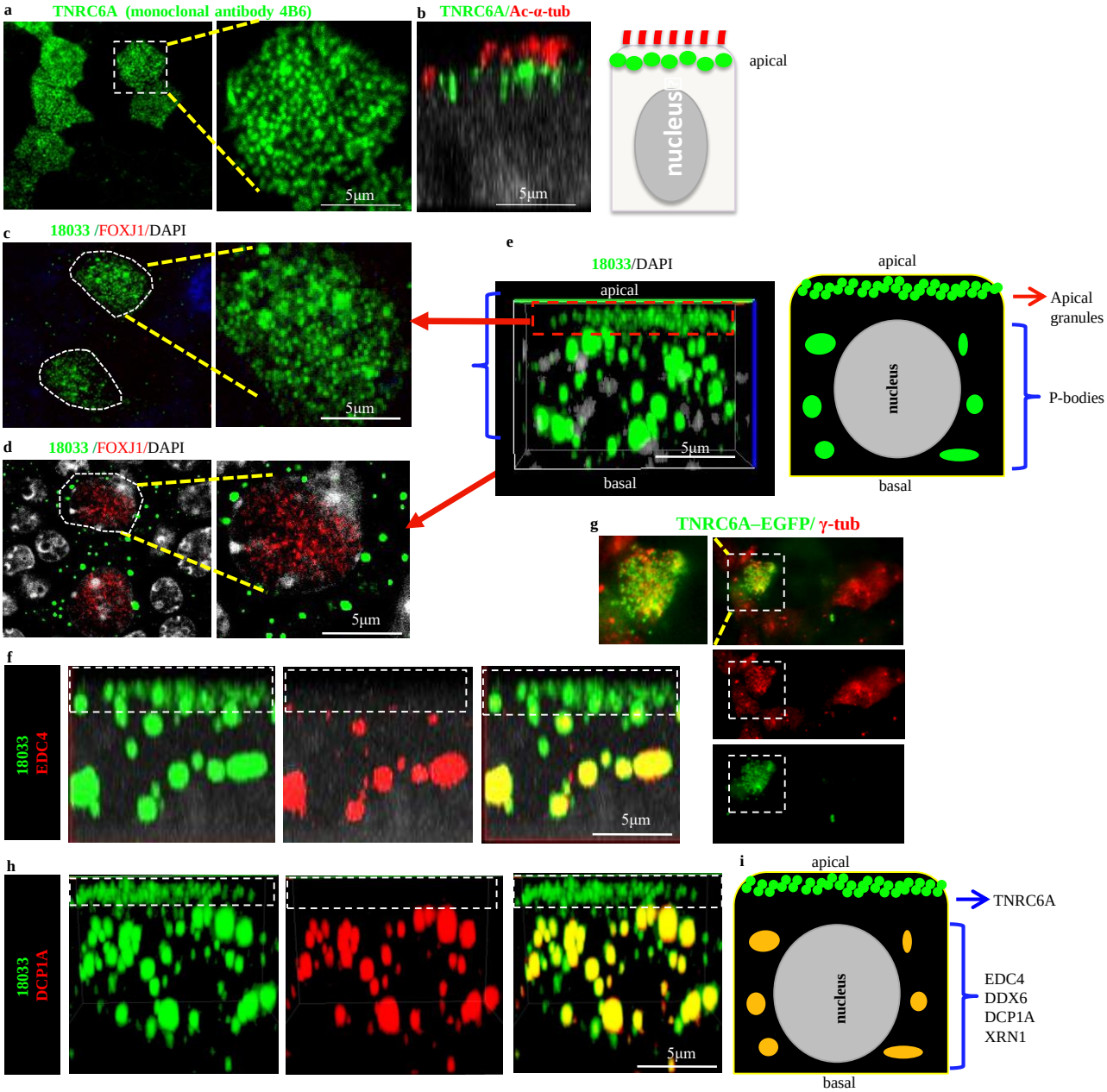

Fig. 2. TNRC6A protein concentrates in apically-localized granules that lack mRNA degradation enzymes (a-i: immunofluorescence, ALI airway epithelial cultures).

a-b) TNRC6A monoclonal antibody (clone#:4B6) detects a novel class of apically-localized granules (highlighted by dashed lines) underneath the multicilia (red, Ac-α-tub). X-Z projection of confocal z-stack images (white: DAPI nuclei).

c) Apically-localized granules detected by human index serum (18033). Dashed lines depict a plane of Z-stack image from the apical area of a MCC.

d) Randomly-localized granules (P-bodies) detected by human index serum. Dashed lines depict a plane of Z-stack image of the same MCC in panel (c) at the level of nuclei (red: FOXJ1; white, DAPI).

e) 3D view of Z-stack images and diagram of a single MCC showing apical (red dashed box) and randomly-localized (P-bodies) granules.

f) Co-staining of EDC4 with human index serum in a single MCC. EDC4 mainly present in P-bodies instead of apical granules (dashed box).

g) TNRC6A-EGFP fusion protein expressed by a lentiviral vector concentrates in apical granules of MCC identified by co-labeling with γ-tub (boxed area) in ALI day3 culture.

h-i) Co-staining of DCP1A with human index serum showing DCP1A largely in P-bodies instead of the apical granules (dashed box) in a single MCC. Diagram depicts distinct components of these granules.

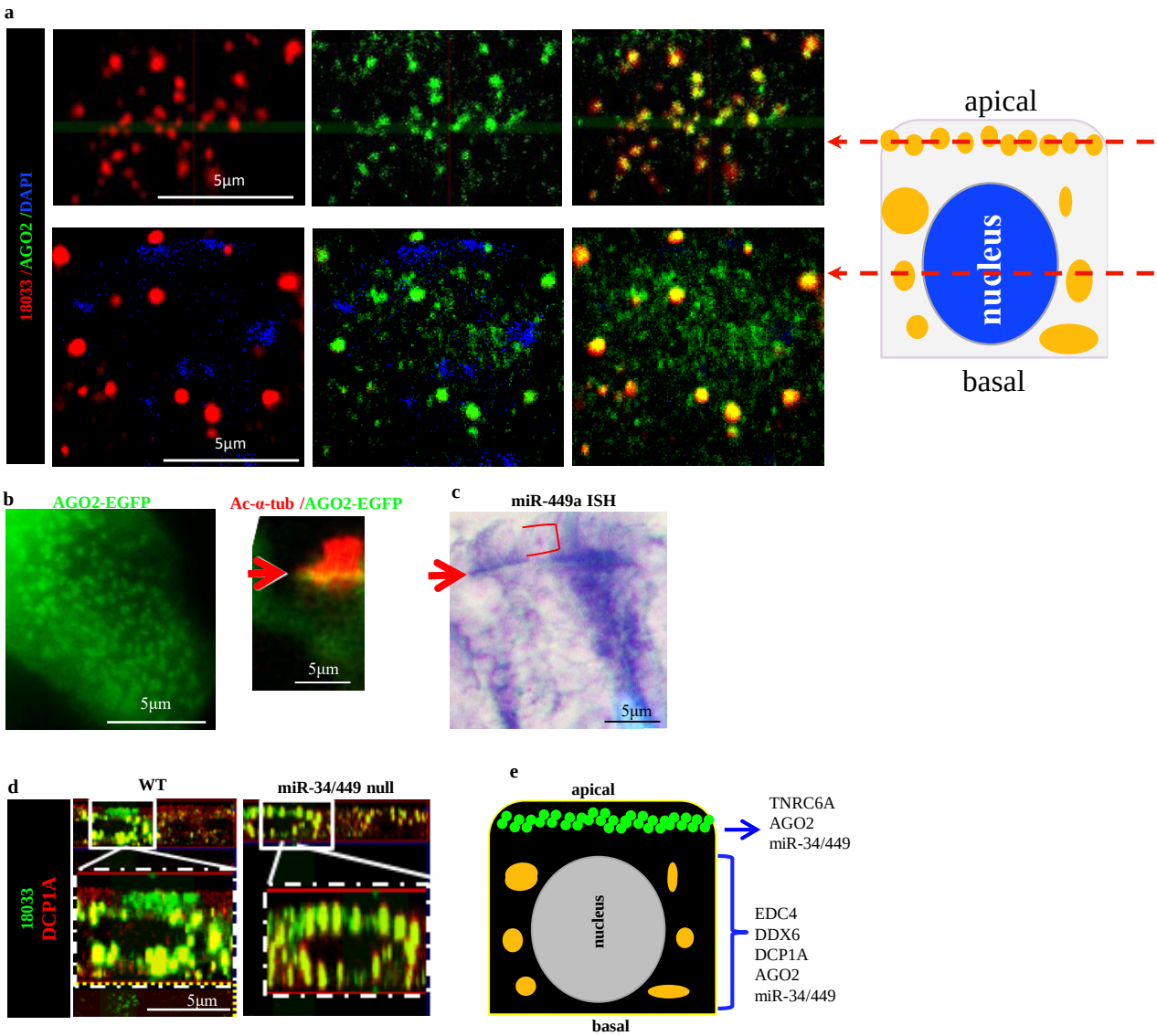

Fig. 3. Apically-localized granules contain AGO2 and miRNAs

a) Co-staining of AGO2 (green, clone 11A9) and TNRC6A (red, human index serum) showing double-labeling in both apical granules and P-bodies within the same MCC (diagram). AGO2 protein is also detected in nuclei of MCC.

b) AGO2-EGFP fusion protein produced by a lentiviral vector in MCC differentiated in ALI cultures form apical granules underneath the emerging cilia (red, Ac-α-tub, red arrow point to concentrated AGO2-EGFP fusion protein underneath cilia).

c) In situ hybridization (ISH) showing miR-449a enriched in apical area of MCCs (red arrow) underneath the cilia (red bracket).

d) Co-staining of DCP1A(red) with human index serum (green) in ALI day 4 cultures from control airway progenitors showing abundant apical granules (single-labeled green) and P-bodies (double-labeled yellow) in MCCs. MCCs from miR-34/449 null (miR-34/449 triple KO) cultures showing less apical granules

e) Diagram depicts the distinct components of these granules.

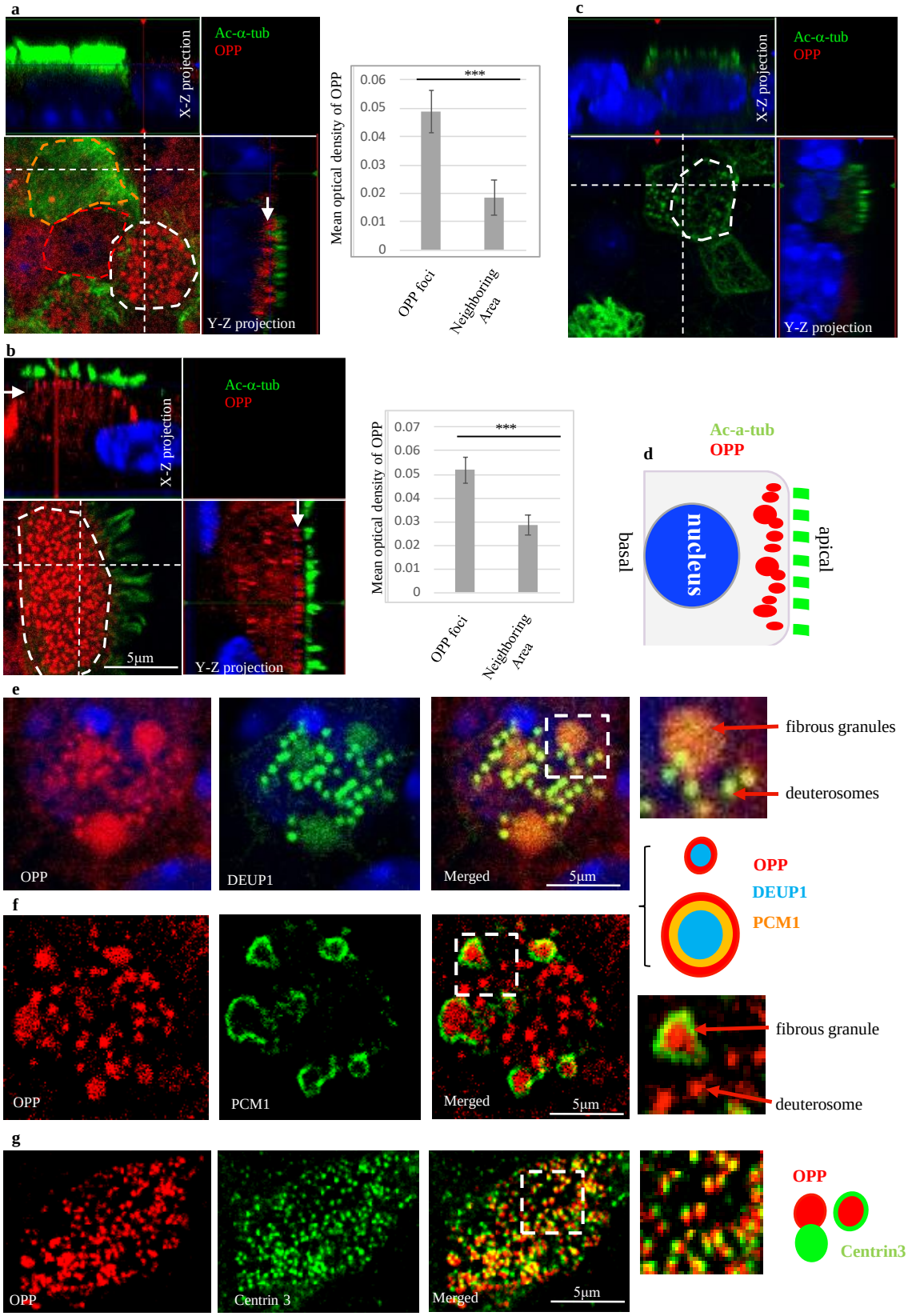

Fig. 4. Newly-synthesized proteins are concentrated in fibrous granules, deuterosomes and apical granules adjacent to centrioles.
a) Newly synthesized proteins labeled with OPP (red) and cilia (green, Ac-α-tub). OPP signal concentrated in apically localized foci of immature mouse MCCs (with shorter and less cilia, white dashed line), but not in mature mouse MCCs (full grown cilia, brown dashed line) and other cell types (red dashed line). The mean optical density of OPP positive foci and neighboring area in total, OPP foci in 30 immature MCCs from three independent cultures were analyzed (Image J software).
b) Similar pattern observed in human immature MCCs.
c) OPP signal abolished by pretreatment of cycloheximide, a protein synthesis inhibitor.
d) Illustration of OPP positive foci in the apical area of both human and mouse immature MCCs.
e-g) OPP foci (red) are present in deuterosomes (marked by DEUP1 staining), or fibrous granules (marked by PCM1) are adjacent or overlapping centrioles (marked by Centrin3). Diagrams depicting the relationship of these components with the small and large OPP foci.
Images in e, f, g: A plane of Z-stack images from the apical area of a single MCC. ***:P<0.0001.

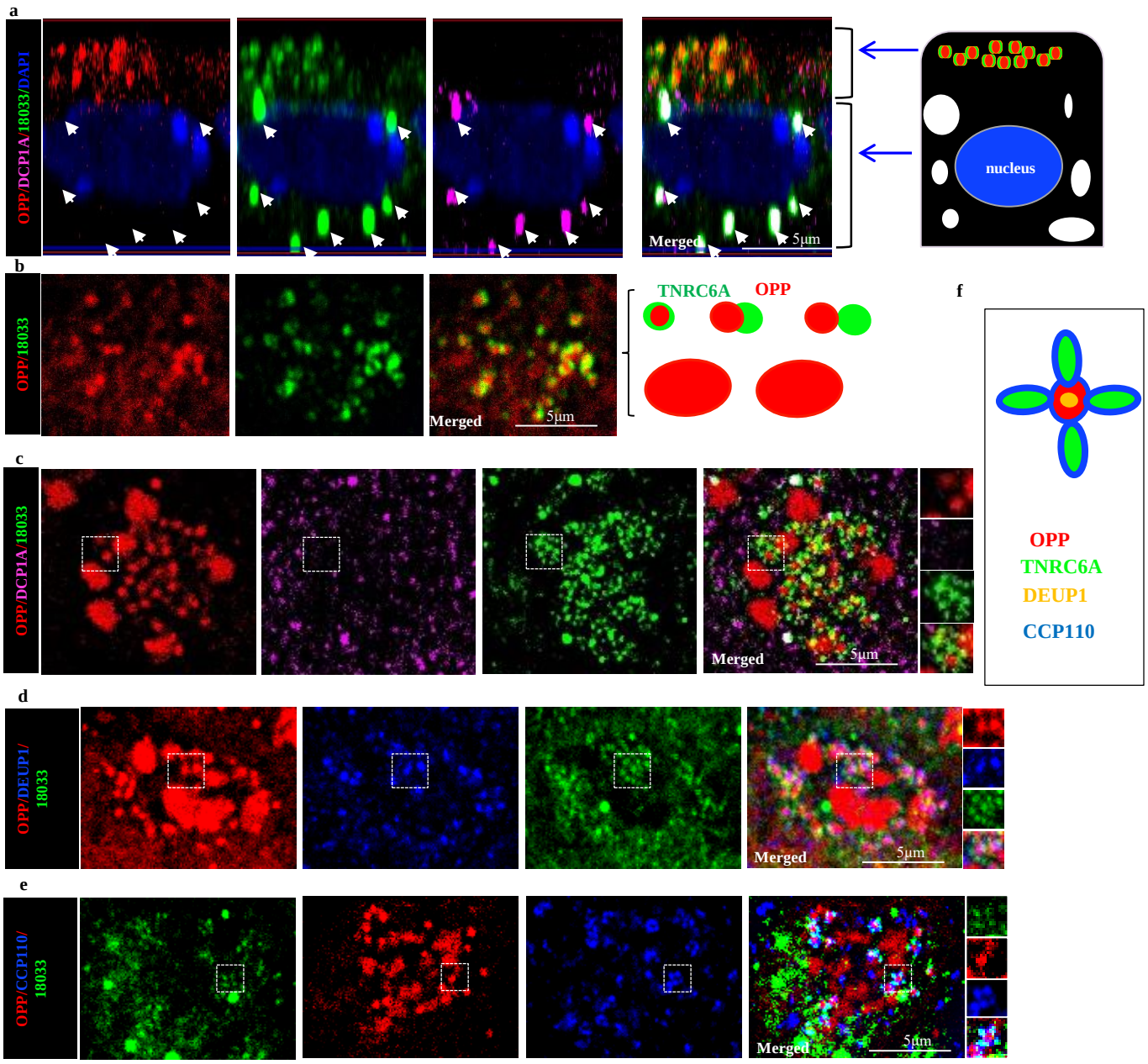

Fig. 5. Newly synthesized proteins are highly concentrated within or adjacent to apically-localized TNRC6A positive granules in ALI day 3 cultures.
a. IF-co-staining of OPP (red, newly-synthesized proteins) with DCP1A (pink) and human index serum (green, 18033) showing OPP concentrated in apical TNRC6A positive granules, but not in DCP1A positive P-bodies of the same MCC. 3D view of Z-stack images of a single MCC.
b. Apical TNRC6A-positive granules (green) overlap or are tightly abutting OPP foci (red, A plane of Z-stack image of the apical region of single MCC). Schematics depicting the TNRC6A-interaction with smaller OPP foci but not with the larger OPP foci (see in c,d).
c, d, e. In some MCCs, TNRC6A positive granules surround OPP foci which is also DEUP1 positive. DCP1A signals do not overlap with TNRC6A or OPP. Deuterosome-associated TNRC6A positive granules co-localize with procentrioles marked by CCP110 staining. A plane of Z-stack image of apical region of single MCC in all images.
f. Schematics of the patterns of expression during centriole amplification. OPP (smaller foci), TNRC6A, DEUP1, CCP110.

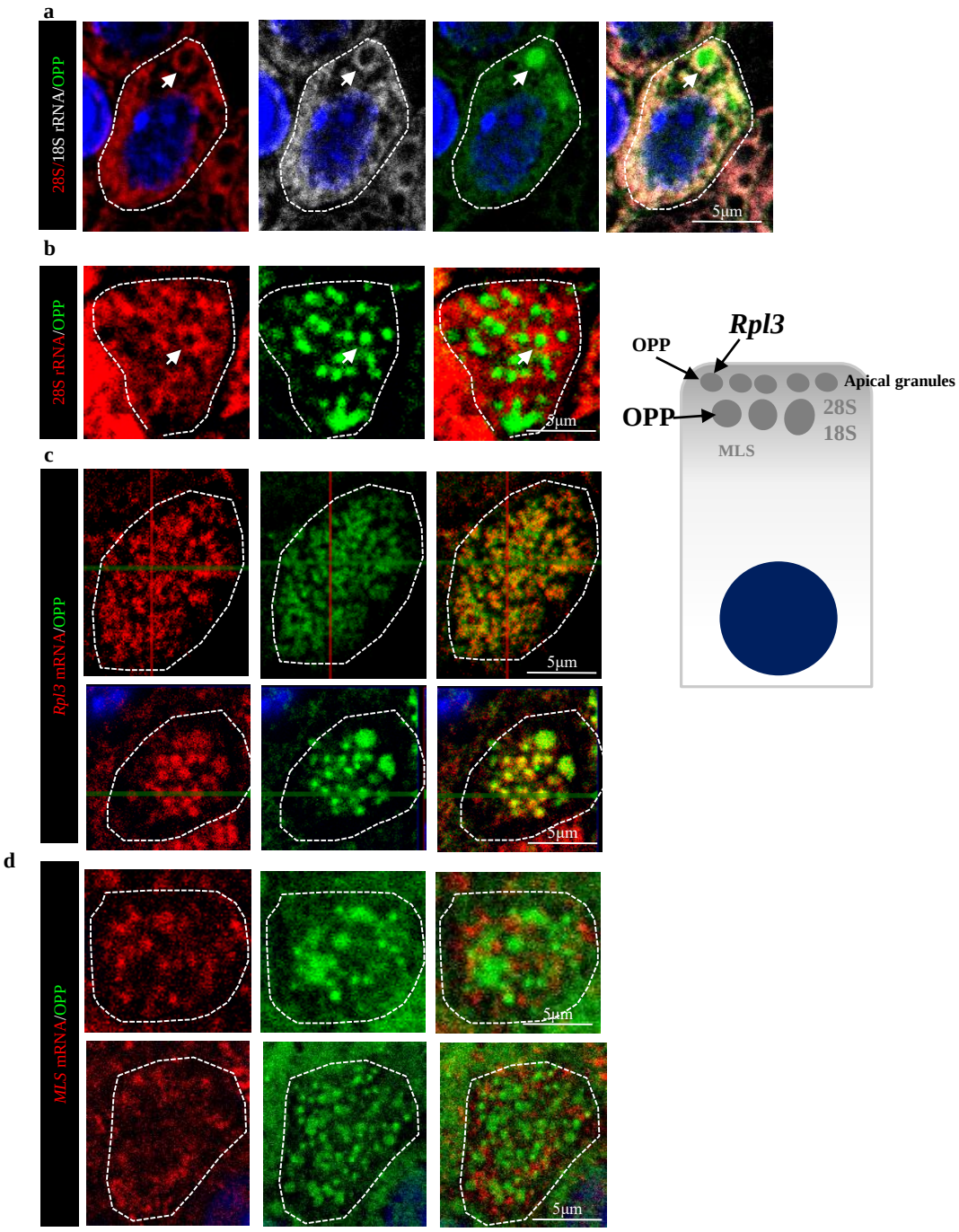

Fig. 6. rRNAs and mRNAs for the ribosomal proteins are associated with OPP positive foci in differentiating MCCs in ALI at Day 3 cultures. RNAs detected by smFISH. A plane of Z-stack image of the apical region of a single MCC shown in each panel**.** Diagram (right) summarizing findings**.**
a-b) 18s and 28s rRNA (white arrow head) are found surrounding OPP foci.
c) Top panel: *Rpl3* mRNA is highly concentrated in OPP foci of the smaller more homogeneous apical granules (Tnr6a-containing). Bottom panel: Larger more heterogenous OPP foci also co-label with *Rpl3* but to a smaller extent.
d) RNA transcribed from the mitochondrial L-strand DNA does not overlap with OPP foci.

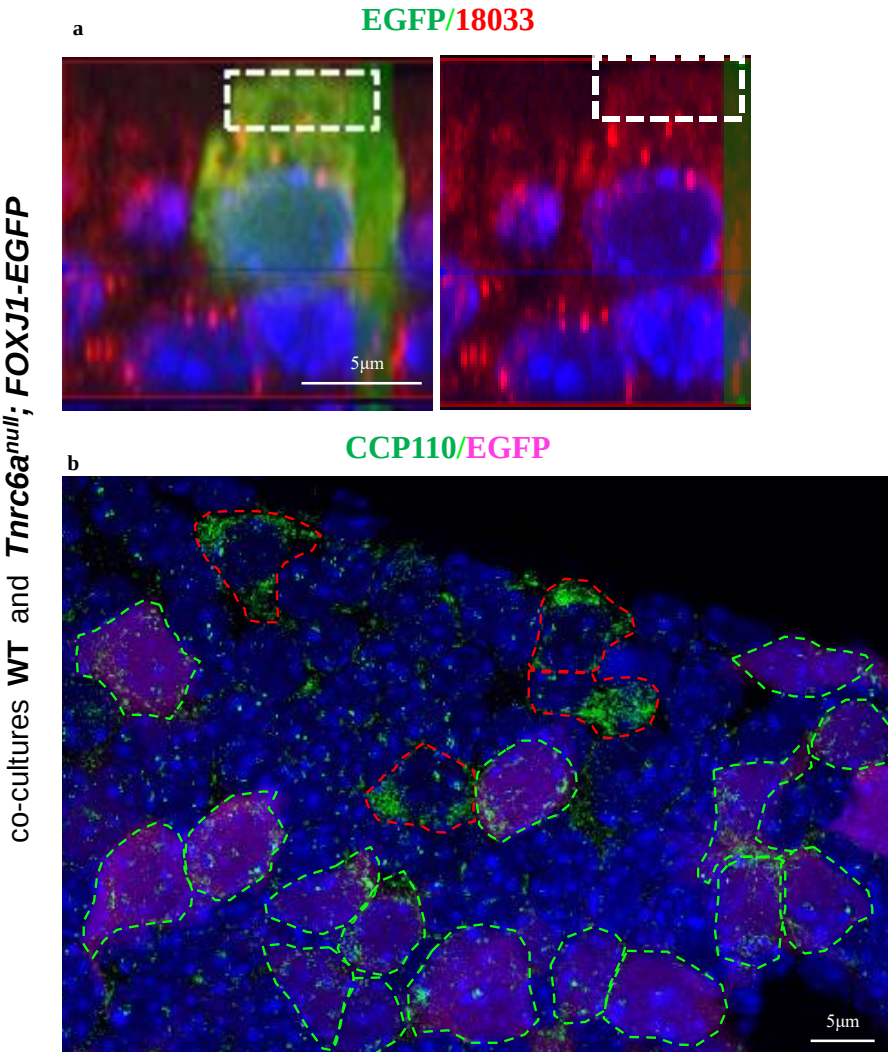

Fig. 7. Disruption of *Tnrc6a* expression leads to the loss of apical granules and a significant reduction of CCP110 protein.
a) *Tnrc6a* null mutant MCCs are marked by FOXJ1-EGFP (green), human index serum (red) stains both apical granules and P-bodies. However in these mutants apical granules are absent (area outlined by dashed lines) due to loss of Tnr6a.
b) CCP110 protein detected by IF staining of co-cultures of *Tnrc6a* null mutant MCCs (marked by FOXJ1-EGFP, pink, outlined by green dashed line) with WT control cells (outlined by red dashed line). CCP110 is nearly absent in *Tnrc6a* null MCCs.

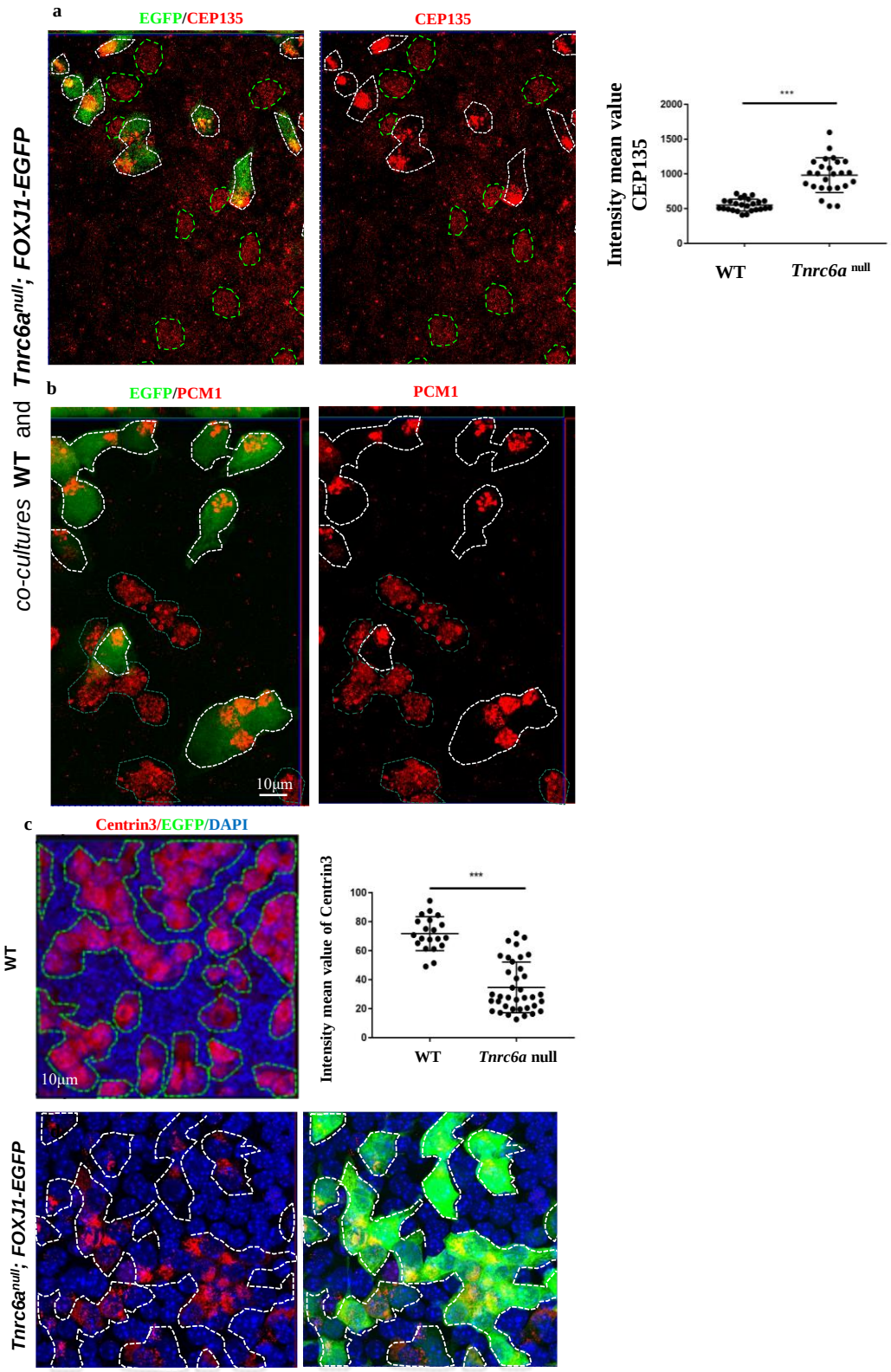

Fig. 8. Defective centriole amplification in *Tnrc6a*-deficient cells .

a, b) CEP135 or PCM1 proteins (red) were detected by IF staining of co-cultures of *Tnrc6a* mutant MCCs (marked by FOXJ1-EGFP, green, outlined by white dashed line) with WT control cells (outlined by green dashed line) differentiating in ALI interface cultures .

c) IF detection of Centrin3 protein (red) in wild type (top panel, dashed lines) and *Tnrc6a* mutant MCCs differentiating in ALI interface cultures (bottom panel, dashed lines, visualized in green by FOXJ1-EGFP expression). Marked decrease in centrin 3 expression in mutant MCCs. The mean optical density of IF signaling (Intensity mean value) was quantified using Image J software. In total, IF staining signal of 30 MCCs from three independent cultures (n=3) were quantified. ***: P<0.0001.

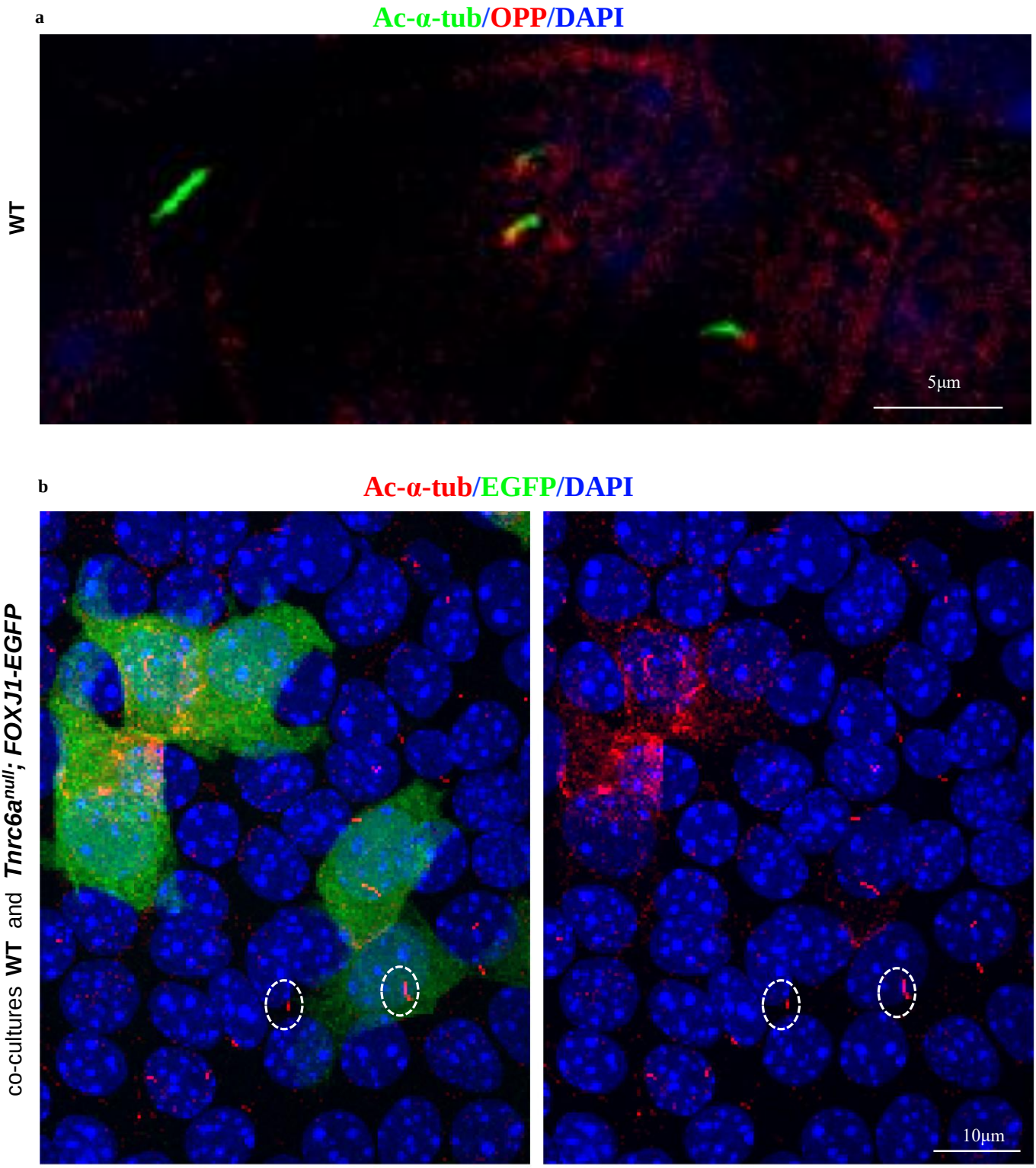

Fig. 9. Disruption of *Tnrc6a* does not prevent primary cilia from forming. IF of ALI airway epithelial cultures at day3
a) WT ALI airway epithelial cultures: newly-synthesized proteins (red, labeled by OPP) are concentrated in foci at the base of primary cilia (green).
b) Co-culture of WT and Tnrc6a null; FOXJ1-EGFP cells a ALI day3 : *Tnrc6a* null cells marked by FOXJ1-EGFP (green) showing no significant defect in primary cilia marked by Ac-α-tub staining (red).

Supplementary Table 1. Genes most downregulated in *Tnrc6a* null lungs

Symbol	Raw intensity *array hybridization*	*p-value*	Fold changes *(Mutant/WT)*	Predicted miR-34/449 *binding site*	*association with cilia structure or function*	*references*
Tnrc6a	1316.98	2.19E-04	0.15	+		
Rnf213	151.14	2.53E-02	0.34	+		
Itpripl2	402.46	8.10E-03	0.45	+		
Nmur1	545.31	8.95E-02	0.51		localize to primary cilia	Omori Y, et al., 2015
Spef2	19.03	7.19E-02	0.54		primary ciliary dyskinesia.	Sironen A, et al., 2011
Itgal	395.25	3.08E-02	0.56	+		
Ankrd49	398.45	1.29E-02	0.58	+		
Aqp1	15434.49	5.37E-02	0.58		localize to cilia	Badran HH, et al., 2002
Hvcn1	128.90	4.48E-02	0.58			
Iigp1	917.28	8.98E-02	0.58			
Tmem159	2528.96	5.46E-02	0.59			
Cyp2e1	877.46	3.31E-02	0.59			
Fam63b	1030.29	9.56E-02	0.60	+		
Pycard	221.56	2.45E-02	0.60			
Tlr8	112.74	8.01E-02	0.60			
Calcrl	22254.51	4.98E-02	0.60	+	ADM (ligand of calcrl) stimulates ciliary motility	Li HW, et al., 2010
Emr1	280.83	8.76E-02	0.61			
Wfdc6b	7.53	2.30E-02	0.61			
Ace	13535.66	3.53E-02	0.61			
Siglecg	169.32	5.42E-02	0.62			
Hck	1354.42	3.45E-02	0.62			
Ccdc12	44.66	8.18E-02	0.62			
Apol7c	44.31	3.07E-02	0.62			
Usf1	349.93	5.19E-02	0.63	+		
Card6	138.13	3.61E-02	0.63			
Treml4	112.72	3.98E-02	0.63	+		
Ide	863.72	8.60E-03	0.63			
Rsph1	297.69	4.67E-03	0.64		primary ciliary dyskinesia.	Knowles MR, et al., 2014
Rhoq	789.97	3.76E-02	0.64	+		
Dock10	539.34	5.07E-02	0.64			

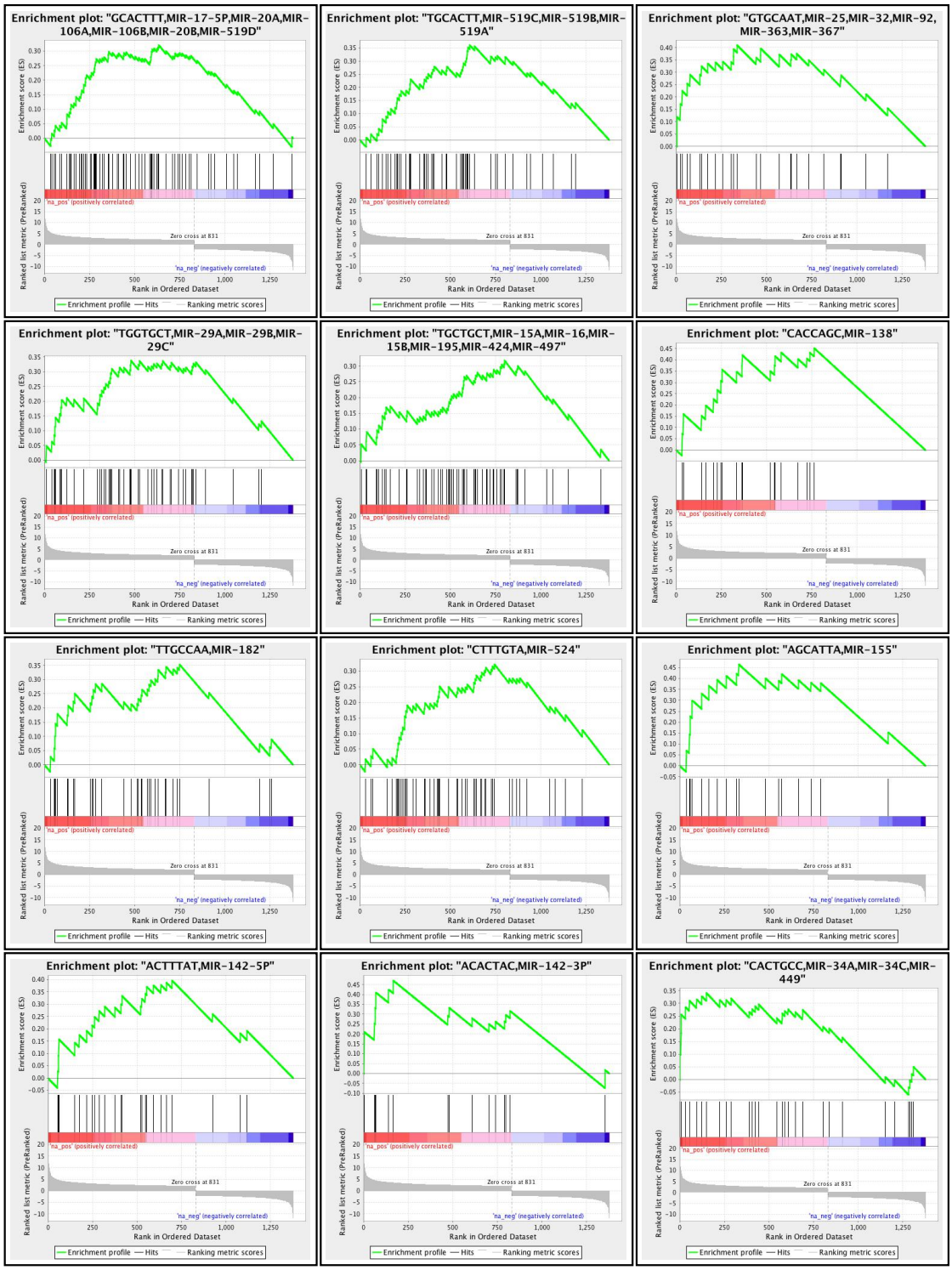

Supplementary Fig. 1 (page 1)**.** miRNA targets are enriched among genes upregulated in *Tnrc6a*^{null} yolk sac.

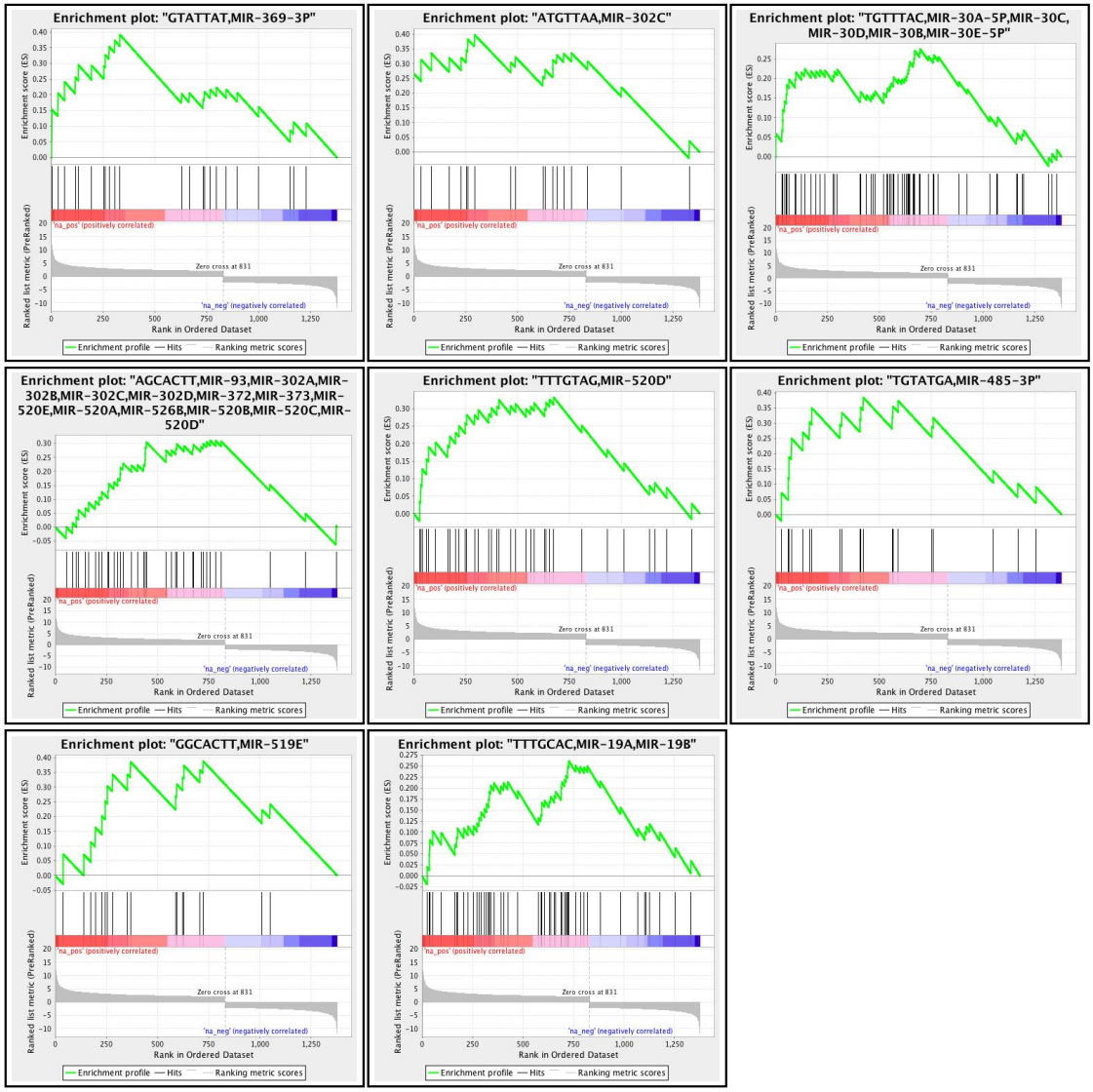

Supplementary Fig. 1 (page 2)**.** miRNA targets are enriched among genes upregulated in *Tnrc6a*^{null} yolk sac.

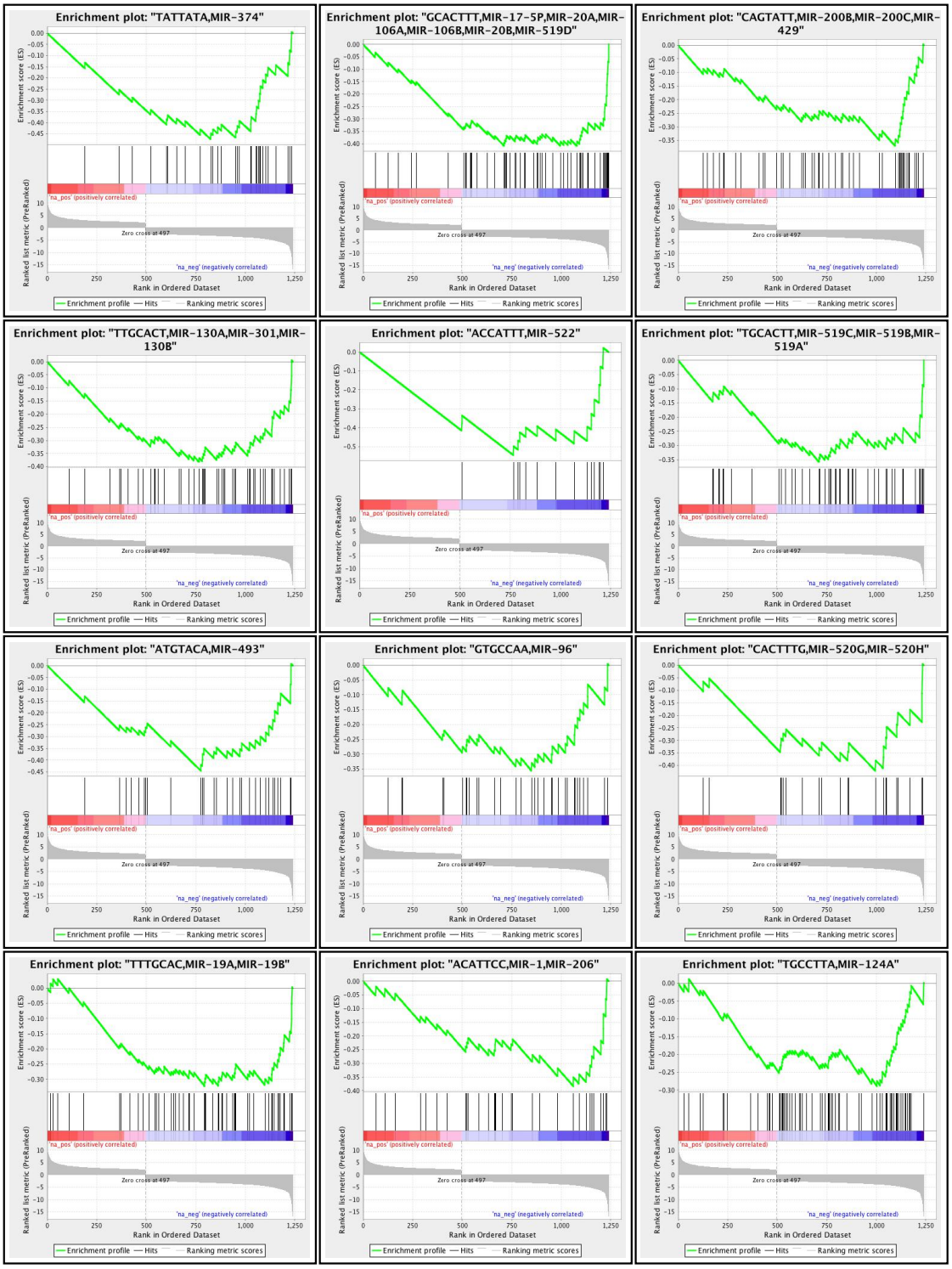

Supplementary Fig. 2 (page 1)**.** miRNA targets are enriched among genes downregulated in E18.5 *Tnrc6a*^{null} lungs

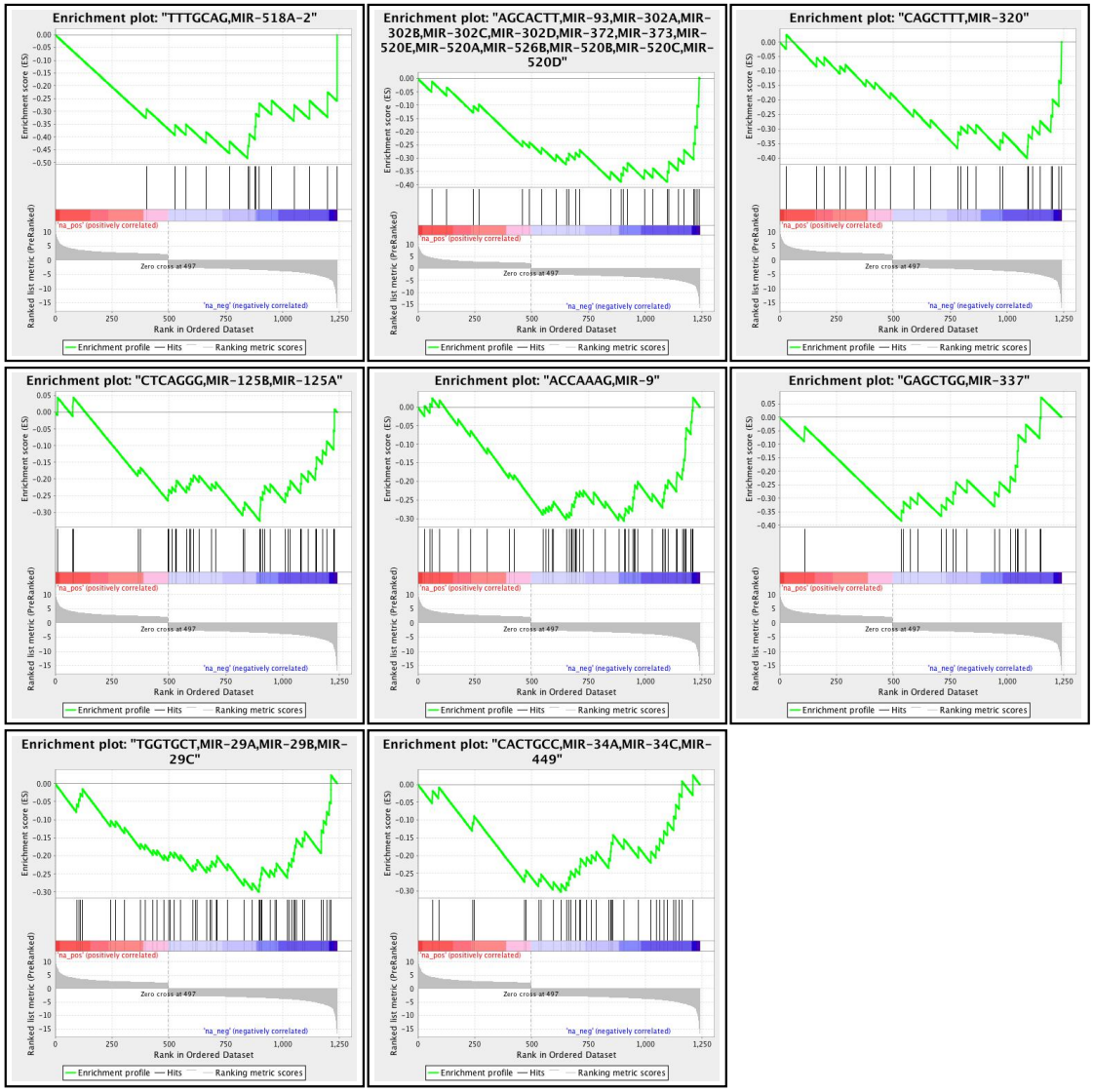

Supplementary Fig. 2 (page 2)**.** miRNA targets are enriched among genes downregulated in E18.5 *Tnrc6a*^{null} lungs

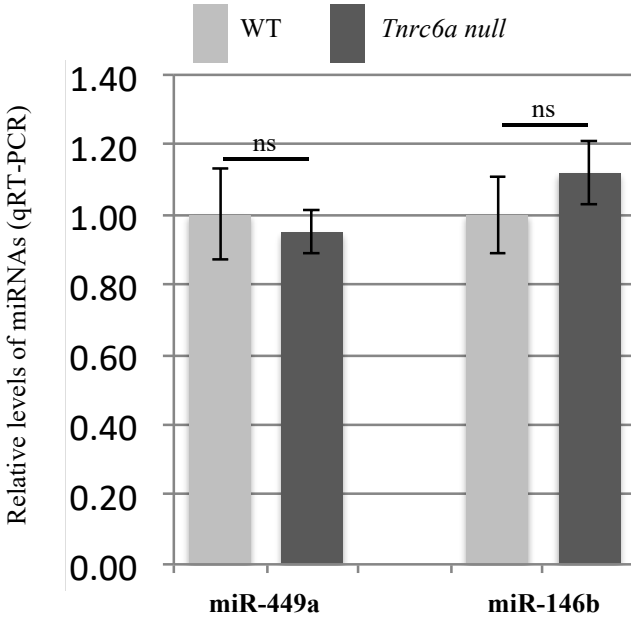

Supplementary Fig. 3. Levels of miR-449a and miR-146b are not altered in *Tnrc6a* ^{null} lungs.

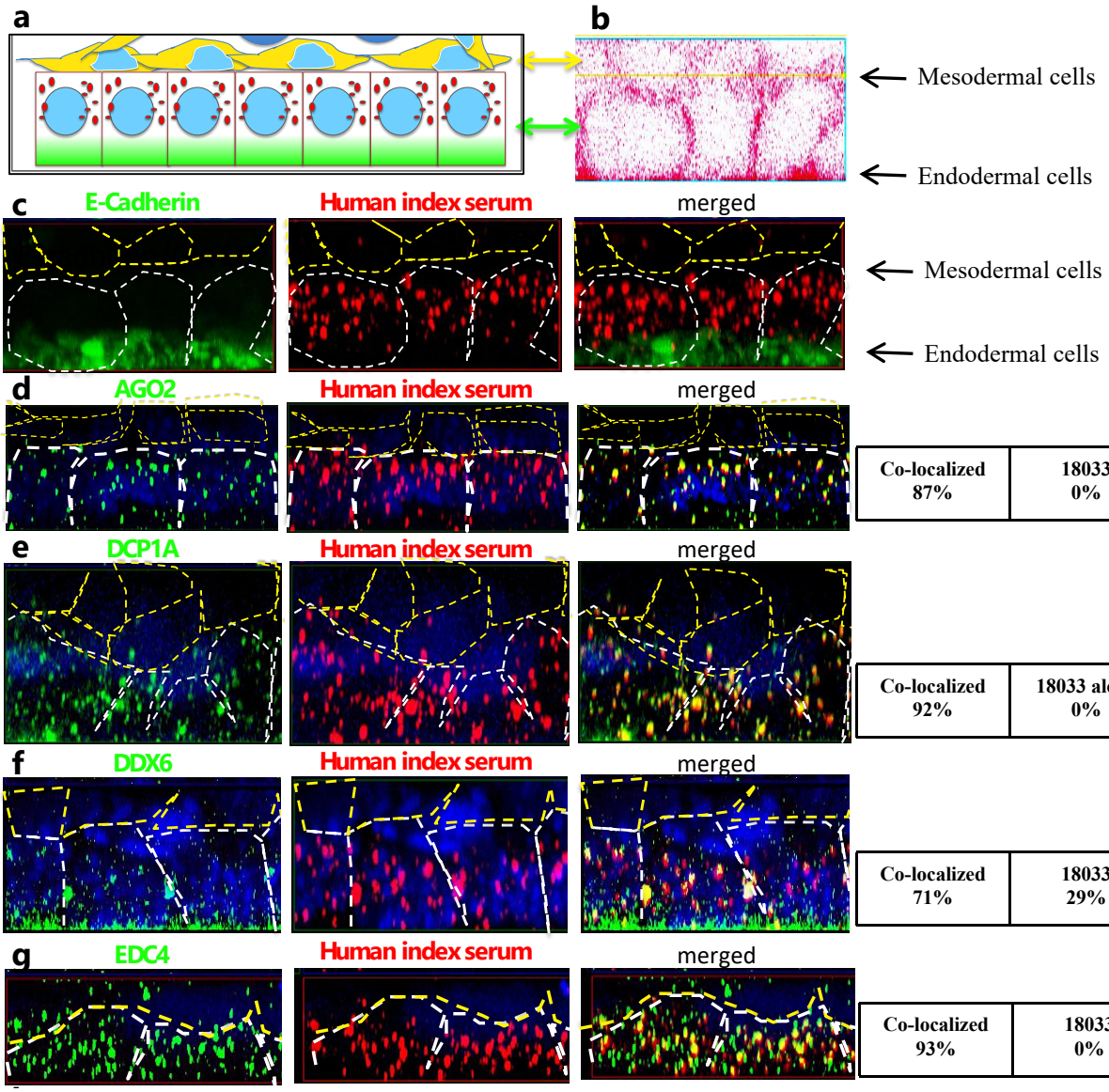

Co-localized	18033	AGO2 alone
87%	0%	13%

Co-localized	18033 alone	DCP1A alone
92%	0%	8%

Co-localized	18033	DDX6 alone
71%	29%	0%

Co-localized	18033	EDC4 alone
93%	0%	7%

Supplementary Fig. 5. TNRC6A proteins concentrate in P-bodies containing AGO2 and enzymes for mRNA degradation in E9.5 mouse yolk sac.
a) Schematics of endodermal and mesodermal (mesenchymal/hematopoietic) cells in E9.5 mouse yolk sac. The expected pattern of E-cadherin staining in endodermal cells where TNRC6A expression is highly enriched is represented in green; Red dots represent typical P-bodies.
b) Y-Z maximum intensity projection confocal image of phalloidin staining signal in three endodermal cells (bottom) and mesodermal cell (top)
c). Y-Z maximum intensity projection images of E-cadherin and TNRC6A (human index serum) co-staining showing large number of P-bodies in endodermal cells.
d-g) Y-Z maximum intensity projection images of co-staining of AGO2 (d), DCP1A (e), DDX6 (f), EDC4(g) and with TNRC6A (human index serum).
Cell boundaries in (c-g) are outlined by dashed lines based on the pattern of phalloidin shown in b.

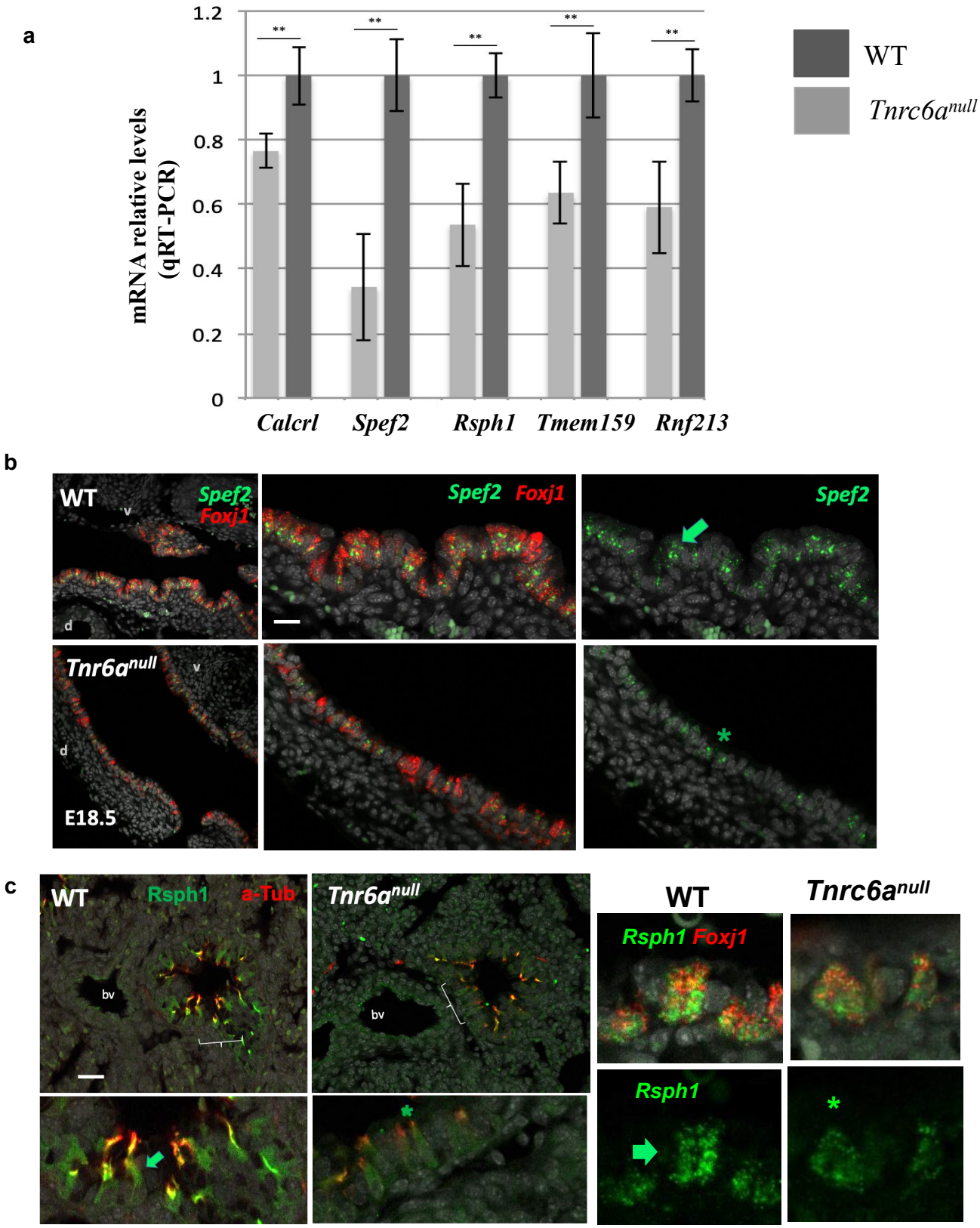

Supplementary Fig. 4. miR-34/449 targets are downregulated in Tnrc6a^{null} lungs. (a) qRT-PCR confirmation of gene targets of miR-34/449 downregulated in *Tnrc6a*^{null} lungs initially detected in our transcriptome analysis (n=3 per group). (b) *Spef2* and *Foxj1* dual in situ hybridization (ISH, RNAscope) showing strong *Spef2* signals (arrow) in MCCs of WT reduced (*) in MCCs of *Tnrc6a*^{null} (representative large airway from both groups: d, dorsal; v, ventral). (c) Rsph1-acetylated a-Tubulin double immunofluorescence showing strong Rsph1 signals in WT MCCs (arrow bottom left) reduced in *Tnrc6a*^{null} airways (* bottom right). Right panel: Double ISH of *Rsph1-Foxj1* confirming strong Rsph1 cytoplasmic signals in WT MCCs decreased in mutant MCCs . (b, c) representative images of n=2 lungs per group. Bars in b, c = 12um and 15 um, respectively.

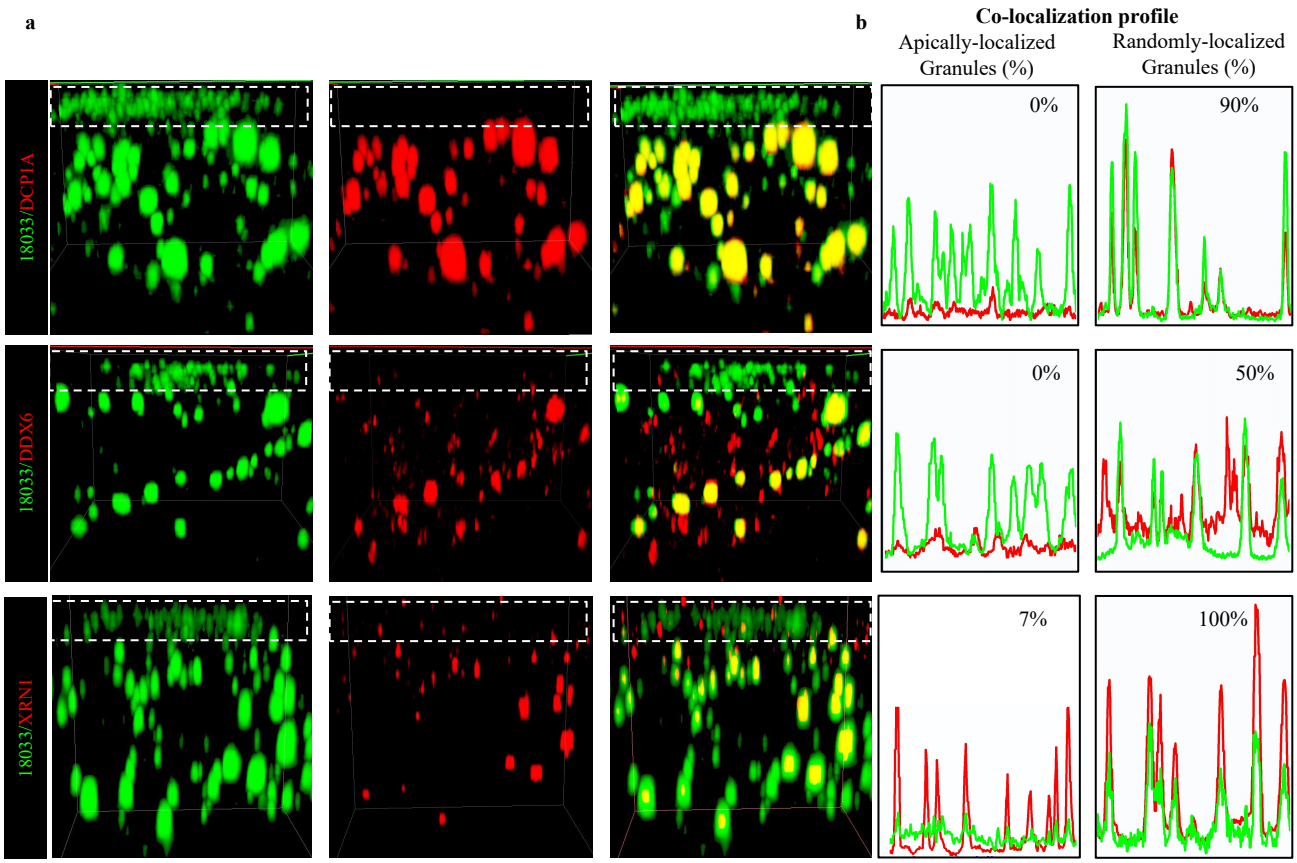

Supplementary Fig. 6. Apical granules lack enzymes for mRNA degradation.

a) Each panel represents a 3D image of confocal Z-stack images of a single MCC in culture. Apically localized granules are highlighted by dashed lines. TNRC6A stained with human Index serum (18033). DCP1A, DDX6 and XRN1 are concentrated in randomly-localized granules (P-bodies). However, DCP1A and DDX6 are undetectable in apically granules. XRN1 are present in small number of apically granules at low levels.

b) Co-localization profile of apically- localized or randomly- localized granules (P-bodies) within the same MCC indicating the different concentration of these proteins in these two classes of granules. Percentage of granules with double labeling signal.

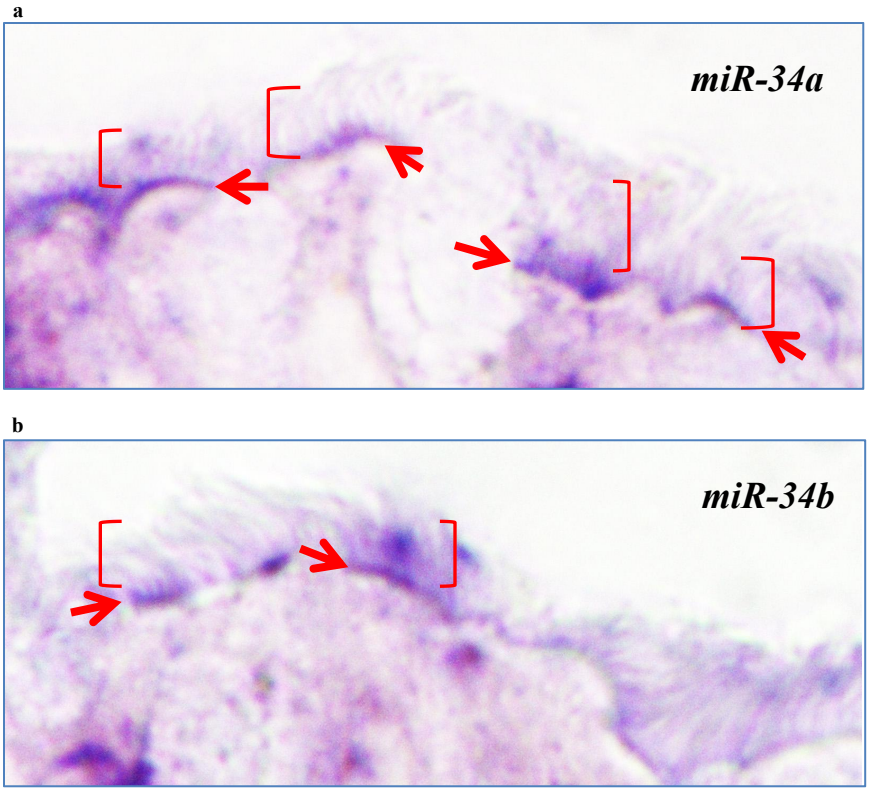

Supplementary Fig. 7. Apically-enriched ISH signal of miRNAs in multiciliated cells of airways in vivo.
a-b) In situ hybridization of miR-34a and miR-34b. Apically-localized signals (arrows) underneath multicilia (bracket)

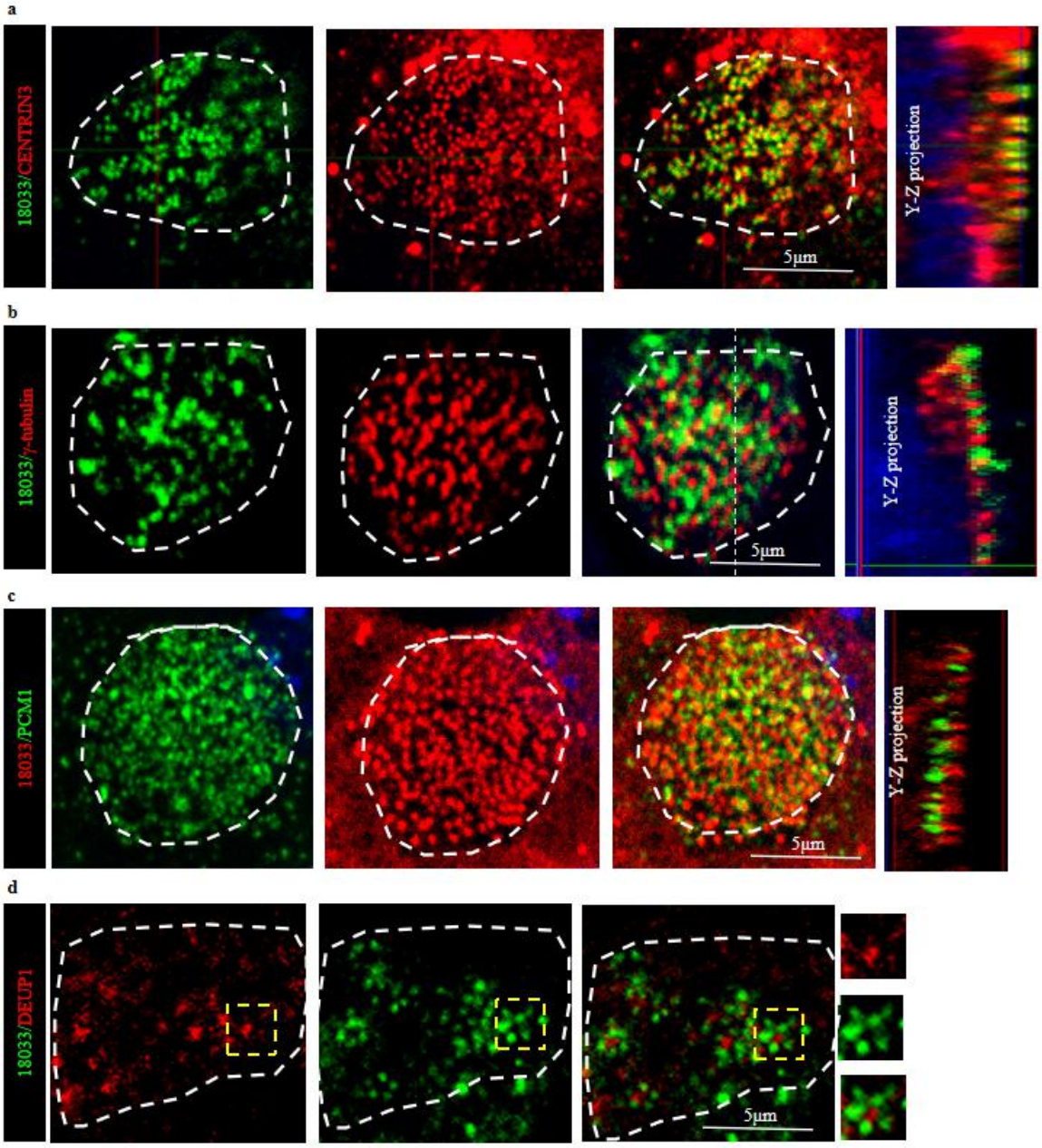

Supplementary Fig. 8. Apical TNRC6A positive granules are adjacent to centrioles. Co-staining of TNRC6A (green or red, human index serum, 18033) with Centrin 3 (red, a), γ-tubulin (red, b), PCM1 (green, c) and DEUP1 (red, d). A plane of Z-stack image of apical region of single MCC is shown in each panel.

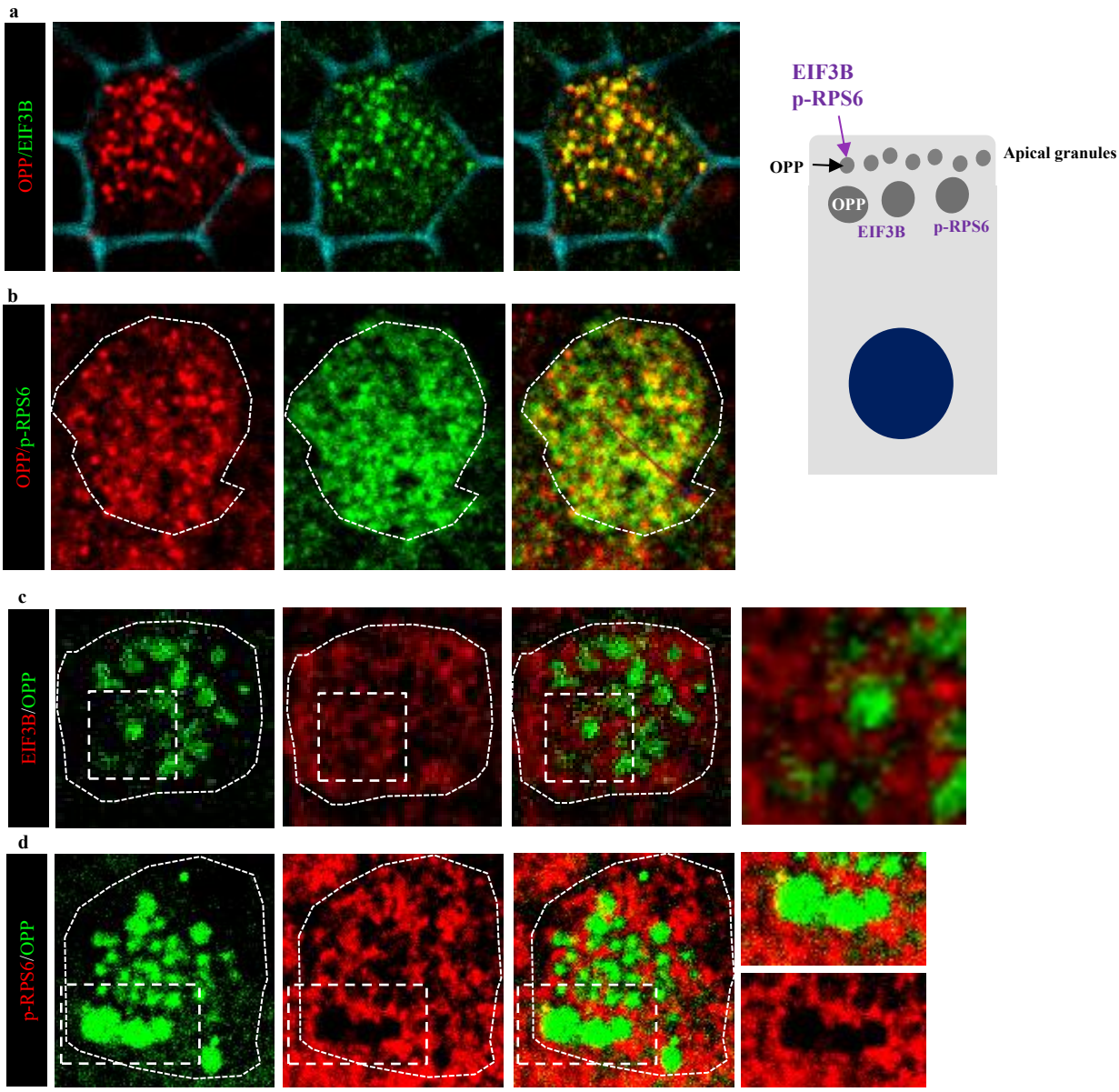

Supplementary Fig. 9. Translation initiation factors are closely associated with apical OPP foci. All panels: confocal images of a single MCC in airway ALI culture. Diagram (right) summarizing findings.
a, b) Translation initiation factors (EIF3B and p-RPS6) (green) overlap with OPP (red) in smaller more homogenously-shaped apical granules (expected to contain TNRC6A). Phalloidin stained cell membrane depicts apical region of MCC.
c, d) By contrast immediately below these regions where large OPP foci are found, EIF3B and p-RPS6 proteins (red) were present in a non-overlapping pattern (high magnification panel on the right enlarged from the boxed area).

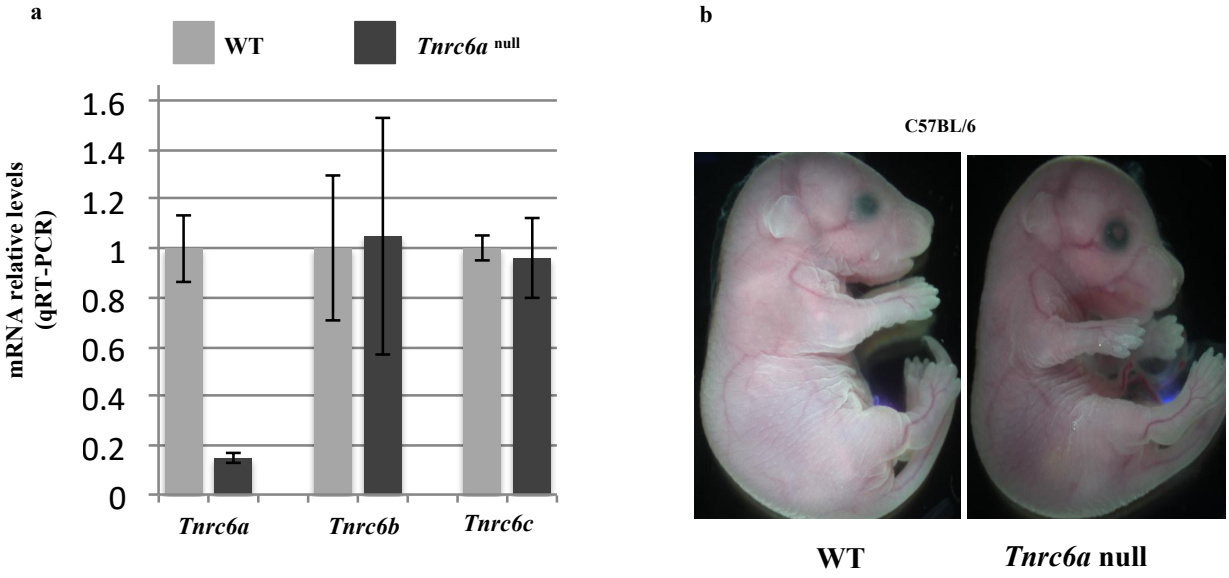

Supplementary Fig. 10.
a) Disruption of *Tnrc6a* expression in *Tnrc6a* ^{null} lungs results in no compensation by *Tnrc6b* and *Tnrc6c* expression.
b) No gross abnormalities were observed in *Tnrc6a* ^{null} embryos at E18.5.

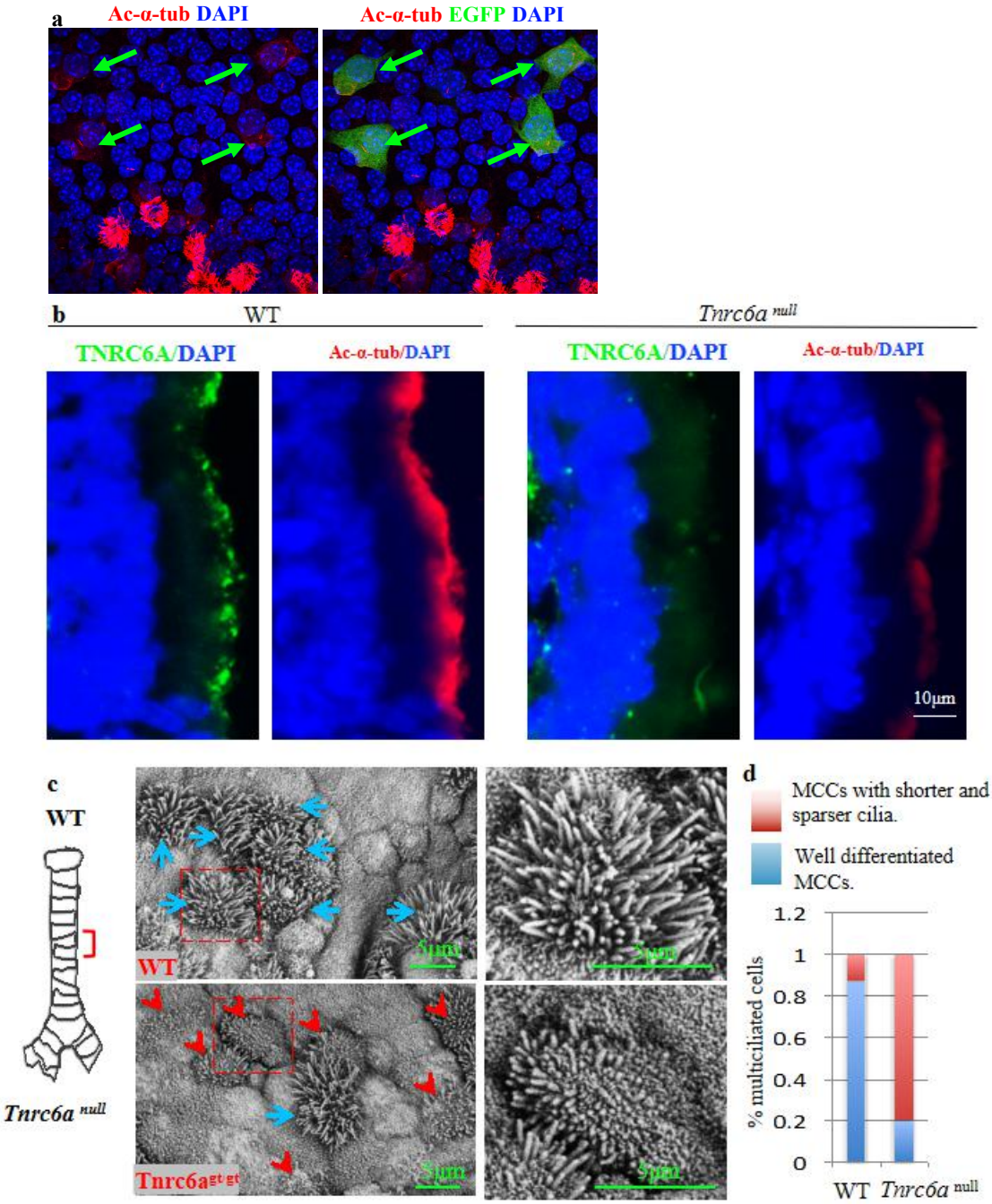

Supplementary Fig. 11. Disruption of *Tnrc6a* results in defective multicilia formation.
a) Tnrc6a mutant cells marked by FOXJ1-EGFP (green) and co-cultured with WT control cells fail to form multicilia marked by Ac-α-tub
b) Co-IF staining of TNRC6A (green, monoclonal antibody 4B6) and Ac-α-tub (red) of wild type or *Tnrc6a*$^{gt/gt}$ airways.
c) Scanning electron microscopy of trachea of wild type or *Tnrc6a* null mice (right panels are enlarged images of highlighted areas by dashed lines); defective (red arrow head) and well differentiated (light blue arrow) multiciliated cells in WT and mutant trachea.
d) Percentage of multiciliated cells with short and sparse cilia in WT and *Tnrc6a* null tracheas (n=2, $p<0.01$).

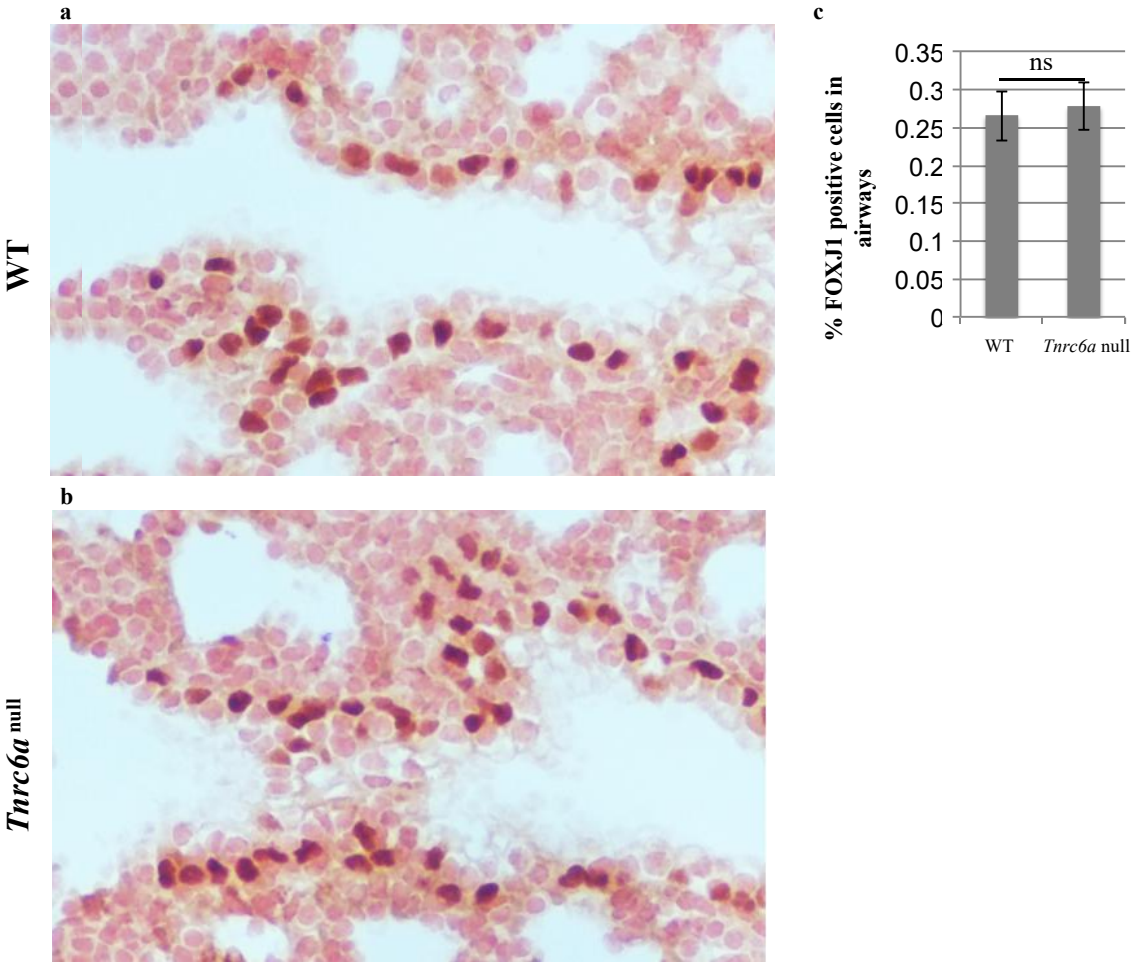

Supplementary Fig. 12. No differences in FOXJ1 expression is detected in wild type or *Tnrc6a null* airways.
a-b) FOXJ1 staining in E18.5 wild type and *Tnrc6a* null airways.
c) Percentage of FOXJ1 positive cells in the airways of wild type and *Tnrc6a* null embryos.